

1 **NFAT5 induction by the tumor microenvironment enforces CD8 T cell** 2 **exhaustion**

3 Laure Tillé^{1*}, Daniela Cropp^{1*}, Gabrielle Bodley¹, Massimo Andreatta^{1,2,3}, Mélanie Charmoy¹, Isaac
4 Crespo^{1,2,3}, Sina Nassiri^{1,3}, Joao Lourenco³, Marine Leblond¹, Cristina Lopez-Rodriguez⁴, Daniel E.
5 Speiser¹, Santiago J. Carmona^{1,2,3}, Werner Held¹, Grégory Verdeil¹

6

7 1 Department of Oncology UNIL CHUV, University of Lausanne, Switzerland.

8 2 Ludwig Institute for Cancer Research, University of Lausanne, Lausanne, Switzerland.

9 3 SIB Swiss Institute of Bioinformatics, Lausanne, Switzerland.

10 4 Immunology Unit, Department of Experimental and Health Sciences, Universitat Pompeu Fabra,
11 Barcelona, Spain.

12 * Co-first authors

13 *Correspondence:* Grégory Verdeil, Department of Oncology, University of Lausanne, Biopole 3, Ch.
14 des Boveresses 155, CH-1066 Epalinges, Switzerland. E-mail: gregory.verdeil@unil.ch

15 *Acknowledgement:* We thank Hana Zdimerova for editing the manuscript, Dr Ping-Chi Ho and Dr
16 Thierry Walzer for suggestions about the project and Patrick Reichenbach for technical counseling. This
17 work was funded by the University of Lausanne, and grants from the Max Cloëtta Foundation (GV), the
18 Swiss National Science Foundation (GV: 310030_182680, WH: 310030B_179570), ISREC institute
19 (DC), the Swiss cancer league (GV).

20 *Author contributions:* L.T, D.C, WH and G.V conceived and designed the experiments. L.T, D.C, M.C,
21 GB, M.L and G.V performed the experiments. J.L analyzed the scRNA-seq data and M.A, S.C and I.C
22 performed bioinformatic analysis. C.L.R provided CD4-Cre NFAT5^{fl/fl} mice. L.T, D.C and G.V prepared
23 the figures and wrote the manuscript with input from all authors. D.E.S, W.H, C.L.R, S.C significantly
24 reviewed the manuscript.

25 Running title: NFAT5 regulates T cell exhaustion in tumors

26 **Abstract**

27 Persistent exposure to antigen during chronic infection or cancer renders T cells dysfunctional. The
28 molecular mechanisms regulating this state of exhaustion are thought to be common in infection and
29 cancer, despite obvious differences in their microenvironments. We discovered that NFAT5, an NFAT
30 family member lacking an AP-1 docking site, is highly expressed in exhausted T cells from murine and
31 human tumors and is a central player in tumor-induced exhaustion. While NFAT5 overexpression
32 reduced tumor control, NFAT5 deletion improved tumor control by promoting the accumulation of
33 tumor-specific CD8⁺ T cells that expressed less TOX and PD-1 and produced more cytokines
34 particularly among precursor exhausted cells. Conversely, NFAT5 had no effect on chronic infection-
35 induced T cell exhaustion. Mechanistically we found that TCR triggering induced NFAT5 expression
36 and that hyperosmolarity stimulated transcriptional activity of NFAT5. We propose that NFAT5 takes
37 over NFAT1/2 to promote exhaustion specifically in tumor-infiltrating CD8⁺ T cells.

38

39 **Introduction**

40 CD8 T cells can actively recognize and eliminate tumor cells. However, CD8 tumor-infiltrating
41 lymphocytes (TILs) are mostly dysfunctional, commonly referred to as exhausted. Exhausted CD8 T
42 cells responding to chronic infection and cancer show high expression of multiple inhibitory receptors,
43 reduced effector functions and are not able to efficiently control pathogens or tumors¹. The exhaustion
44 state is strongly related to the constant presence of antigen, resulting in continuous triggering of the
45 TCR², but the composition of the local microenvironment further influences the gene expression of
46 exhausted CD8 T cells³.

47 Despite the tremendous progress in cancer immunotherapy during the past years⁴, a large fraction of
48 patients' cancers remains, or becomes, therapy resistant. Understanding the molecular mechanisms that
49 regulate T cell exhaustion is a first step towards more efficient treatments. Recent studies highlighted
50 the existence of a precursor exhausted T cell (Tpex) population with stem cell-like properties, which
51 can further differentiate into terminally exhausted T cells (Tex) that have cytolytic potential but are short
52 lived. Several transcription factors (TF) such as TOX and NFAT play central roles in the establishment
53 of T cell exhaustion, while others, such as TCF-1, maintain the stemness properties of Tpex^{1, 5, 6}. TOX
54 drives the expression of inhibitory receptors and negatively regulates the production of inflammatory
55 cytokines allowing T cell maintenance in the context of chronic antigen stimulation^{7, 8}. Importantly, it
56 has been shown that TOX is directly regulated by NFAT1 and NFAT2^{9, 10}, which are activated by
57 calcineurin downstream of TCR signaling¹¹. NFAT1 and NFAT2 are required for effective CD8 T cell
58 differentiation into cytotoxic T cells by forming dimers with transcriptional partners such as AP-1¹².
59 However, the overexpression of a constitutively active version of NFAT1 unable to interact with AP-1
60 induces an exhausted phenotype in CD8 TILs¹³. As AP-1 expression in chronically-stimulated T cells is
61 reduced, exhaustion is at least partly induced by NFAT activation in the relative absence of AP-1¹³.

62 A previous transcriptomic analysis of CD8 T cells from tumor-infiltrated lymph nodes (TILN) showed
63 that the NFAT family member NFAT5 is highly expressed in TILN cells¹⁴. In contrast to the classical
64 NFAT proteins, NFAT5 lacks an AP-1 docking site and is not regulated by calcineurin¹⁵. Instead,
65 NFAT5 is triggered by metabolic stress, such as hypertonicity, and regulates the transcription of proteins

66 involved in the maintenance of an adequate osmotic balance in a cell type-unspecific manner¹⁶.
67 However, the activity of NFAT5 varies according to the cell type or the stimulus^{17, 18}. Recent studies
68 found that NFAT5 regulates inflammatory responses in macrophages¹⁹ and CD4 T cells²⁰, but so far
69 there is no report on functional alterations of peripheral CD8 T cells through NFAT5¹⁷.

70 Our study showed that NFAT5 is highly expressed in CD8 TILs from murine and human tumors.
71 Overexpression of NFAT5 dampened CD8 T cell responses against tumor cells, while deletion of
72 NFAT5 further improved CD8 T cell anti-tumor functions without impacting their capacity to
73 accumulate and differentiate. Surprisingly, NFAT5 deletion in CD8 T cells during chronic LCMV
74 infection had no effect on T cell exhaustion and virus control, emphasizing a tumor-specific T cell
75 regulatory role of NFAT5. By deciphering the different stimuli present in the tumor microenvironment
76 (TME), we found that TCR triggering is the main inducer of NFAT5 expression and that
77 hyperosmolarity increases NFAT5 activity in the TME. Therefore, our data established that NFAT5 is
78 a tumor-specific regulator of CD8 T cell exhaustion.

79

80 **Results**

81 **NFAT5 is upregulated in tumor-infiltrating CD8 T cells**

82 NFAT5 was previously found highly expressed in Melan-A-specific CD8 T cells obtained from
83 metastasized lymph nodes¹⁴. To confirm the expression of *NFAT5* in CD8 TILs, we took advantage of
84 publicly available single cell RNA-seq (scRNA-seq) data from mouse B16 melanoma²¹, mouse MC38
85 adenocarcinoma²², human melanoma^{23,24} and human breast cancer²⁵. The CD8 TIL were classified into
86 naïve like, early activated, effector memory, precursor exhausted (Tpex) and terminal exhausted (Tex)
87 CD8 T cell subsets, using ProjectTILs²⁶. *NFAT5* was highly expressed in Tpex and Tex compared to
88 naïve like, early effector and effector memory CD8 TILs in all studies (Fig. 1a, Extended Data Fig. 3).
89 We used the same datasets to identify the most relevant TFs regulating T cell exhaustion by comparing
90 their regulon activity (AUC score) in the different subsets. A regulon represents a gene set regulated by
91 the same transcription factor. The regulon activity of NFAT5 was upregulated in Tpex and Tex. NFAT5
92 is in the top 8 TFs showing statistically significant differences between these two subpopulations
93 compared to the other subtypes, together with Tbet, Runx2 and Bhlhe40 for upregulated regulons (Fig.
94 1b). We further confirmed the upregulation of NFAT5 by quantitative PCR (qPCR) in CD8 T cells
95 sorted from the spleen or tumors of B16 melanoma²⁷ tumor-bearing mice (Fig. 1c) and in human Melan-
96 A-specific CD8 TILN, using circulating EBV-specific or naïve circulating CD8 T cells as controls (Fig.
97 1d).

98 To follow NFAT5 expression at the single cell level, we generated an NFAT5 reporter mouse strain, in
99 which the stop codon in exon 14 of NFAT5 was replaced by a P2A-mCherry cassette (Extended Data
100 Fig. 1a). In these mice, mCherry expression in CD8 T cells correlated with the level of NFAT5 mRNA
101 (Extended Data Fig. 1b). We further confirmed that the introduction of the P2A-mCherry cassette did
102 not alter NFAT5 expression. We compared the NFAT5 protein level in CD8 T cells from WT, NFAT5
103 KO and NFAT5_{mCherry} mice (Extended Data Fig. 1c, d). We did not observe any effect on the viability
104 or breeding capacity, or thymic development, of the NFAT5-mCherry reporter mouse strain (Extended
105 Data Fig. 1e-g). Using this model, we showed that polyclonal CD8 TILs from B16 or MC38 tumors
106 expressed significantly higher levels of NFAT5 compared to CD8 T cells from the tumor-draining lymph

107 node (T-DLN) or the non-draining lymph node (N-DLN) on day 16 post tumor injection (Fig. 1e-f). To
108 define the kinetic of NFAT5 induction in CD8 TILs, we engrafted NFAT5_{mCherry} mice with B16-OVA
109 (Fig. 1g). Seven days post engraftment, endogenous CD8 T cells from the tumor and the LNs expressed
110 similar levels of mCherry. At this time point we transferred activated OT-I-NFAT5_{mCherry} CD8 T cells
111 into some of the tumor bearing mice. Three days after transfer, both endogenous and OT-I CD8 TILs
112 showed an increased level of mCherry, which remained stable for OT-I cells but dropped for endogenous
113 CD8 TILs, while tumor growth was transiently controlled, until day 18 (Fig. 1h). Once tumor growth
114 resumed, we observed a strong increase of mCherry levels in OT-I cells and to a lesser extent in
115 endogenous CD8 TILs. In the absence of OT-I CD8 T cell transfer, B16-OVA tumor growth was not
116 controlled. In this situation, the level of mCherry also increased at day 10 and remained stable at day 14
117 (Fig. 1i). The rapid growth of the tumors did not allow us to measure further time points. Altogether, we
118 found enhanced NFAT5 expression in T_{pex} and T_{ex} CD8 TILs both in human and murine tumors and
119 increasing NFAT5 levels during tumor progression.

120 **NFAT5 overexpression dampens CD8 T cell tumor control.** To test whether high NFAT5 levels in
121 CD8 T cells impact their response against established tumors, we cloned different NFAT5 isoforms that
122 differ in the alternative splicing of the first and last exons, into GFP-expressing retroviral vectors (Fig.
123 S2a) and transduced TCRP1A-luc⁺ CD8 T cells expressing luciferase and a TCR recognizing the P1A
124 epitope expressed by P511 mastocytoma cells^{28, 29}. Adoptive transfer of as little as 10⁴ transduced
125 TCRP1A-luc⁺ CD8 T cells was sufficient to induce tumor regression^{30, 31}. Following the transfer of
126 sorted NFAT5 isoform A, that lacks the Nuclear Export Signal (NES) sequence, overexpressing CD8 T
127 cells into P511 mastocytoma-bearing Rag1^{-/-}B10D2 mice (Fig. 2a-b), we observed reduced tumor
128 control compared to control eGFP-transduced CD8 T cells (Fig. 2c). A similar reduction in tumor control
129 was obtained with NFAT5 isoform D, that contains the NES, while the deletion of the DNA binding
130 domain of NFAT5 restored tumor control (Extended Data Fig. 2). Furthermore, overexpression of
131 NFAT1 CA-RIT, a constitutively active form of NFAT1 unable to bind AP-1, reduced tumor control in
132 a similar extent as NFAT5 (Fig. 2c). In this model we have previously shown a disadvantage of CD8 T
133 cells overexpressing exhaustion-associated genes to sustain in the host, leading to a rapid enrichment of

134 GFP- TCRP1A T cells that do not express our gene of interest^{30, 31}. Therefore, even the slight, but
135 significant, delay in tumor control was a good indicator of NFAT5-mediated impairment of CD8 TIL
136 anti-tumor functions. We did not detect any difference in T cell accumulation by measuring
137 bioluminescence throughout the experiment, suggesting that NFAT5 did not impair the infiltration of
138 CD8 T cells into the tumor (Extended Data Fig. 2). To further characterize their phenotype, we sorted
139 eGFP⁺ CD8 TILs seven days after T cell transfer and performed RNA-seq analysis. Principal
140 component (PC) analysis revealed that NFAT5 and NFAT1 CA-RIT-overexpressing CD8 TILs
141 clustered together, distant from control eGFP-transduced CD8 T cells (Fig. 2d). Most of the
142 differentially expressed genes (n=35), compared to control eGFP CD8 TILs, were upregulated in both
143 NFAT5 and NFAT1 CA-RIT-overexpressing CD8 TILs (Fig. 2e). Within the shared genes we found
144 *Dusp* family phosphatases (2, 5 and 10) as well as *Nr4a1* and *Nr4a3*, which have been associated with
145 the regulation of T cell exhaustion³². Gene Ontology (GO) term analysis revealed similar transcriptomes
146 of both NFAT5 and NFAT1 CA-RIT-overexpressing CD8 TILs, namely signatures associated with cell
147 cycling (chromosome condensation, mitotic regulation), inhibition of MAPK signaling and cell
148 differentiation. Altogether, NFAT5 overexpression in tumor-specific CD8 T cells reduced tumor control
149 through the induction of a transcriptional program similar to that induced by a NFAT1 construct that
150 cannot associate with AP-1.

151 **NFAT5 deletion in tumor-specific T cells improves tumor control**

152 To test whether NFAT5 deletion influenced the tumor response, we crossed CD4-Cre NFAT5^{lox/lox} mice
153 with a P14 TCR transgenic strain, which is specific for the LCMV-derived gp33 epitope. In this model,
154 T cell-specific deletion of NFAT5 does not impair T cell development or alter the peripheral T cell
155 compartment³³. We transferred activated NFAT5^{lox/lox} CD4-Cre^{-/-} (WT) or NFAT5^{lox/lox} CD4-Cre^{+/-}
156 (KO) P14 CD8 T cells into mice bearing subcutaneous gp33-expressing B16 melanoma (B16-gp33)
157 (Fig. 3a). Mice transferred with KO P14 CD8 T cells developed much smaller (and later) tumors
158 compared to the transfer of WT P14 CD8 T cells (Fig. 3b). Seven days after T cell transfer, higher
159 proportions of KO than WT P14 CD8 T cells infiltrated the tumor. Strikingly, KO CD8 TILs produced
160 more IFN- γ , TNF- α and IL-2 upon *ex-vivo* stimulation and expressed less PD-1 than WT P14 CD8 TILs,

161 while CD44 expression was comparable (Fig. 3c), indicating reduced exhaustion of NFAT5 KO CD8 T
162 cells.

163 To decipher the molecular mechanism for the enhanced tumor control by KO CD8 T cells, we performed
164 RNA sequencing on sorted P14 CD8 TILs seven days after transfer. PC analysis revealed that WT and
165 KO CD8 TILs clustered separately (Fig. 3d). We found 458 genes significantly upregulated and 833
166 genes significantly downregulated in KO CD8 TILs (Extended Data Table 1). By comparing the gene
167 signatures to available scRNA-seq data from CD8 TILs^{21, 22, 23, 24, 25}, we found that KO CD8 TILs
168 overexpressed genes found in early activated CD8 TILs, while genes highly expressed in Tex and T_{pex}
169 were downregulated in KO CD8 TILs (Fig 3e). Indeed, several genes previously associated with CD8
170 T cell exhaustion were downregulated in KO cells, including *Cd244a* (2B4), *Entpd1* (CD39), *Pdcd1*
171 (PD-1), *Ikzf2* (Helios) and *Tox* (Extended Data Table 1). Conversely, KO cells overexpressed the
172 cytotoxic molecule Granzyme A, activation-associated genes such as *Tnfrsf4* (4-1BB), *Tnfrsf18* (GITR)
173 and *Ccl5*, genes expressed by T resident memory cells (*Cd69*, *Cxcr6*, *Ccr8*), memory T cells (*Il7r*) or
174 associated with T cell differentiation (*Rora*) (Fig. 3f, Extended Data Table 1). Given the role of TOX
175 in T cell exhaustion^{7, 8, 9, 34}, we assessed whether a reduced TOX expression accounted for the effect of
176 NFAT5 KO. We compared our signature with the one obtained after *Tox* inactivation using GSEA³⁴.
177 We found that genes downregulated upon NFAT5 KO were significantly enriched among TOX-
178 dependent genes and *vice versa* (Fig. 3g). To extend our findings to human T cells, we studied the
179 correlation of NFAT5 expression with exhaustion-related genes in human melanoma TILs, using single
180 cell RNA-seq³⁵. We calculated the Pearson correlation coefficients between *NFAT5* and all detected
181 genes in activated CD8 TILs as judged by *CD44*, *PDCDI* or *TNFRSF4* expression. Consistently, we
182 found that *NFAT5* expression in human TILs positively correlated with *HAVCR2*, *PDCDI* and *TOX*
183 expression. Conversely, *NFAT5* expression negatively correlated with *IL7R*, *GZMA* and *CD69*
184 expression (Fig. 3h). Altogether, NFAT5 KO CD8 TILs expressed less PD-1 and TOX and produced
185 more inflammatory cytokines, resulting in a more efficient tumor control. Furthermore, we found that
186 in both murine and human datasets, NFAT5 plays a major role in the regulation of exhaustion-associated
187 genes.

188 **NFAT5 does not alter the CD8 T cell response to chronic LCMV infection**

189 T cell exhaustion also develops during chronic infection³⁶. We therefore tested whether NFAT5
190 regulated the CD8 T cell response to chronic viral infection. We adoptively transferred mice with naïve
191 WT or KO P14 cells one day prior LCMV clone 13 infection, which causes chronic infection (Fig. 4a).
192 At day 28 post-infection, we found slightly higher proportions of KO P14 cells. Compared to WT P14
193 cells, these cells produced comparable levels of effector cytokines (IFN- γ , TNF- α and IL-2) (Fig. 4c)
194 and only slightly overexpressed PD-1 and CD44. Finally, weight loss during infection, which is
195 indicative of immunopathology, was comparable between mice receiving WT and KO P14 cells (Fig.
196 4b). Altogether, NFAT5 deficiency did not have a significant effect on the CD8 T cell response to
197 chronic LCMV infection, suggesting a tumor-specific role of NFAT5 in T cell exhaustion.

198 **NFAT5 is preferentially expressed in Tpex within CD8 TILs**

199 To understand why NFAT5 inactivation did not restore CD8 T cell function during chronic infection
200 while CD8 TILs function was strongly improved, we performed a more detailed analysis of NFAT5
201 expression in exhausted CD8 T cells. We used available scRNA-seq data from murine CD8⁺ T cells
202 responding LCMV clone 13 infection. Focusing on the various CD8 T cell subsets, we found that
203 NFAT5 levels were high in Tpex compared to Tex and to the other subtypes. Overall, NFAT5 levels
204 were lower in P14 cells responding to chronic infection than P14 TIL subsets (Extended Data Figure 3b,
205 Fig. 1a). To confirm these data, we took advantage of our NFAT5_{mCherry} reporter mouse strain crossed
206 to the P14 TCR transgenic mice (P14-NFAT5_{mCherry}). P14-NFAT5_{mCherry} cells were either transferred
207 into B16-gp33 melanoma-bearing mice or into WT mice one day prior infection with LCMV clone 13
208 (chronic) or Armstrong (acute) strains. After seven days in B16-gp33 tumors and 8 or 28 days in LCMV
209 infected mice, we measured the mCherry levels in Tpex and Tex P14 CD8 T cells (Fig. 5a-b). To
210 compare the two models, mCherry expression was normalized to the fluorescence of endogenous CD8
211 T cells. NFAT5 expression was higher in Tpex than in Tex after chronic infection at day 28, while the
212 level was low in both populations after acute infection and at day 8 after chronic infection. Strikingly,
213 at day 14 (seven days post-transfer) the fold change of NFAT5 in Tpex from CD8 TILs was higher than
214 in the chronic infection on day 28 (Fig. 5a, b). We further confirmed these data by using OT-I-

215 NFAT5_{mCherry} CD8 T cells transferred into B16-OVA-bearing mice (Fig. 5c). We followed mCherry
216 expression in Tpex and Tex from CD8 TILs on day 10, 14, 16 and 23 post-tumor injection
217 (corresponding to day 3, 7, 11 and 16 post-OT-I transfer). Initially, the levels in Tpex and Tex were
218 similar at day 10 but preferentially increased in Tpex on day 14 and 18, reaching a maximum on day 23.
219 In conclusion, we established that NFAT5 expression levels are lower in CD8 T cells in the context of
220 acute and chronic infection as compared to CD8 TILs and that NFAT5 levels are higher in Tpex
221 compared to Tex, with an increasing level as tumor progresses.

222 **NFAT5 inactivation impacts strongly Tpex CD8 TILs**

223 Considering the differential NFAT5 expression in Tpex and Tex, we looked at the effects of NFAT5
224 KO on these populations. After chronic infection, we did not observe significant changes neither in the
225 proportions of the two populations (Fig. 5d) nor in absolute numbers. IFN- γ production, as well as the
226 level of PD-1, were also similar (Fig. 5e). In contrast, NFAT5 KO resulted in a decreased proportion,
227 but similar number of Tpex CD8 TILs compared to WT CD8 TILs, while both the proportion and
228 number of Tex increased seven days after T cell transfer in-tumor bearing mice (Fig. 5f). Furthermore,
229 NFAT5 KO Tpex expressed lower levels of PD-1 and TOX and included higher frequencies of IFN- γ -
230 producing cells as compared to WT CD8 TILs, while Tex, although in greater number, were less
231 impacted by the NFAT5 deletion (Fig. 5g). We established that NFAT5 KO led to an increased number
232 of tumor-specific CD8 T cells. This effect was mostly mediated through Tpex, which displayed a less
233 exhausted phenotype and differentiated more efficiently into cytotoxic Tex, resulting in improved tumor
234 control.

235 **NFAT5 expression is driven by TCR signaling in CD8 TILs**

236 To explore how NFAT5 is triggered in CD8 TILs, we tested various stimuli known to be associated with
237 the TME or described to regulate NFAT5 expression and/or activity. To test the effect on NFAT5
238 expression in CD8 T cells, we cultured P14-NFAT5_{mCherry} splenocytes for 72h in hyperosmotic and/or
239 hypoxic conditions with or without TCR stimulation. TCR stimulation with gp33 peptide or anti-CD3
240 and anti-CD28 antibodies drastically increased mCherry levels. Separately, the addition of NaCl or KCl

241 to the cell culture medium lead to a dose-dependent (380mOsm vs 420mOsm) increase of mCherry
242 levels. Strikingly, combining TCR triggering and hypertonic medium (with NaCl or KCl) led to maximal
243 mCherry expression. On the other hand, hypoxic conditions (0,5% O₂) did not induce mCherry
244 expression alone or in combination with TCR triggering or high osmolarity (Fig. 6a).

245 To assess the importance of TCR triggering on NFAT5 induction in the TME, we co-transferred P14-
246 and OT-I-NFAT5_{mCherry} CD8 T cells into mice bearing two B16 tumors expressing the respective
247 epitopes recognized by these TCRs; gp33 or OVA (Fig. 6b). We observed a TCR/peptide-MHC
248 dependence of mCherry expression for P14 and OT-I CD8 TILs in both TME (Fig. 6c-d). Interestingly,
249 OT-I CD8 T cells, which have a higher affinity to their cognate peptide than P14 CD8 T cells (K_d OT-
250 I/SIINFEKL = 5.9 μ M³⁷ versus P14/gp33 = 3.5 μ M³⁸), showed an even stronger induction of mCherry
251 in both the T-DLN and the tumor site of B16-OVA (Fig. 6c, d, Extended Data Fig. 4). Therefore, TCR
252 stimulation in the TME is necessary to induce NFAT5 expression. Since TCR stimulation leads to
253 Ca²⁺/calcineurin-induced NFAT1 or NFAT2 activation¹³, we wondered to which extent NFAT5
254 expression is dependent on this TCR-Ca²⁺/calcineurin-NFAT axis. The calcineurin inhibitor FK506 is
255 widely used to block calcineurin targets such as NFAT1 and NFAT2. As in previous experiments, we
256 transferred pre-activated P14-NFAT5_{mCherry} into B16-gp33-bearing mice. Mice received FK506 either
257 the first three days (first phase) or the fourth to sixth day (second phase) post T cell transfer (Fig. 6e).
258 The inhibition of calcineurin targets by FK506 partially decreased mCherry expression when FK506
259 was administrated during the first phase, while it had no effect during the second phase on mCherry
260 expression (Fig. 6f). This effect was not observed in the T-DLN and N-DLN, showing a TME-specific
261 effect of calcineurin inhibition on NFAT5 expression in the first phase (Extended Data Fig. 4).
262 Strikingly, PD-1 and TOX levels showed similar trends, with a drastic decrease when FK506 was given
263 during the first phase, but a mild decrease in the second phase (Fig. 6f), suggesting NFAT-independent
264 regulation of PD-1 and TOX at later stages.

265 It was previously established that the concentration of K⁺, but not Na⁺ is increased in the TME of
266 melanoma compared to the serum or healthy tissue from both mouse and human³⁹. We questioned
267 whether the ionic imbalance induced by K⁺ in the TME could participate in the transcriptional regulation

268 of NFAT5 as we observed *in vitro*. We overexpressed KCNA3, a potassium channel enabling T cells to
269 equalize intracellular potassium concentration in its wild type form (KCNA3), or in a non-conducting
270 form (KCNA3 mutant) in activated P14-NFAT5_{mCherry} CD8 T cells and transferred them into B16-gp33
271 tumor-bearing mice. After 17 days, KCNA3-overexpressing P14 CD8 TILs showed a trend for
272 decreased mCherry expression compared to the KCNA3 mutant control (Extended Data Fig. 4).

273 Beside the level of expression, the capacity of NFAT5 to act as a transcription factor is subject to further
274 regulation^{16,40}. To test how different stimuli can impact the DNA binding capacity of NFAT5, we cloned
275 a NFAT5 binding motif, the tonicity-responsive enhancer (TonE), into a luciferase-expressing lentiviral
276 vector and transduced Jurkat cells, which express endogenous NFAT5 (Extended Data Fig. 4a). Culture
277 of Jurkat cells (stably expressing the NFAT5 reporter construct) in the presence of NaCl or KCl induced
278 luciferase activity in a dose-dependent manner. In contrast, TCR triggering, hypoxia, ROS inducers
279 (Butyl-Hydroperoxid) or cytokine stimulation (TGF- β) did not upregulate NFAT5 activity, suggesting
280 a dominant role for hypertonic stress to induce NFAT5 activity (Fig. 6g).

281 Altogether, TCR stimulation and hypertonicity regulated the NFAT5 transcriptional level, while only
282 the osmolar changes increased NFAT5 activity *in vitro*. *In vivo*, TCR triggering is the main driver of
283 NFAT5 transcription.

284

285

286 **Discussion**

287 We showed that NFAT5, an unconventional member of the NFAT family, plays a crucial role in the
288 regulation of tumor-induced T cell exhaustion. NFAT5 was expressed in CD8 TILs in various cancers
289 (melanoma, adenocarcinoma, breast cancer) and in different species (mouse and human). In our study,
290 overexpression of NFAT5 in tumor-specific CD8 T cells limited their anti-tumor response, while its
291 inactivation strongly increased tumor control. NFAT5 deletion had a different effect depending on the
292 subtype of CD8 TILs. NFAT5 KO T_{pex} showed increased production of cytokines and decreased levels
293 of PD-1 and TOX, while their absolute number remained constant. In contrast, we found higher
294 frequencies and absolute numbers of T_{ex}, but the effect of NFAT5 deletion on the function of these cells
295 was limited. These effects correlated with the NFAT5 expression levels in T_{pex} and T_{ex} CD8 TILs,
296 with significantly higher NFAT5 expression in T_{pex} compared to T_{ex}. RNA-seq analysis confirmed
297 that NFAT5 KO CD8 TILs expressed genes associated with early activation, with a signature that
298 correlated with the one measured in TOX-KO CD8 TILs. We observed that the overexpression of
299 NFAT5, or of a mutated form of NFAT1 unable to cooperate with AP-1 and involved in the regulation
300 of exhaustion, has similar effects on the behavior and transcriptional program of tumor-specific T cells¹³.
301 Since TOX is a direct target of NFAT1 and ^{29, 34}, our data suggest that a part of the effect of NFAT5
302 inactivation is mediated via the reduced level of TOX in T_{pex}. The TME inhibits NFAT activation
303 through glucose deprivation or accumulation of lactic acid^{41, 42}. This goes in parallel with an increased
304 osmotic stress related to dead cell accumulation^{39, 43}. We hypothesize that, at this stage, NFAT5 takes
305 over classical NFAT to enforce an NFAT-induced transcriptional program and thus stabilizes the
306 expression of exhaustion-associated genes.

307 Interestingly, the inactivation of NFAT5 in CD8 T cells during chronic infection with LCMV clone 13
308 did not improve viral control nor restore CD8 T cell functions. This argues in favor of a tumor-specific
309 role of NFAT5, explained by a higher expression level of NFAT5 in CD8 TILs compared to CD8 T
310 cells from chronic LCMV infection. Furthermore, our comparison was done at day 7 post-transfer for
311 CD8 TILs, which does not correspond to the highest NFAT5 levels in T_{pex} CD8 TILs.

312 NFAT5 is primarily described to regulate osmolarity-regulated genes, which were not differentially
313 expressed in our experiments. However, NFAT5 activity is not limited to the regulation of this panel of
314 genes. In macrophages, expression of NFAT5 drives a pro-inflammatory phenotype, which further
315 supports T cell-mediated tumor control¹⁹. Interestingly, while NFAT5 drives the expression of tonicity-
316 responsive genes in macrophages cultured in a hypertonic environment, it drives IL-6 production when
317 stimulated with LPS⁴⁴. Therefore, NFAT5 regulates gene expression in a context- and cell type-
318 dependent manner. Similarly, while NFAT5 drives the expression of tonicity-responsive genes in T cells
319 cultured in a hypertonic environment⁴⁵, it was shown to negatively regulate IFN- γ production in CD4 T
320 cells *in vitro*²⁰.

321 We demonstrated that the main inducer of NFAT5 in T cells *in vivo* is TCR stimulation, at least in part
322 through calcineurin activation, suggesting a regulation by classical members of the NFAT family. This
323 regulation was more important during the first phase post T cell transfer (until day 3), while in a later
324 phase (until day 6), calcineurin inhibition had a reduced effect on NFAT5 expression, but also on PD-1
325 and TOX levels. In addition to TCR stimulation, hypertonicity is a major inducer of NFAT5 *in vitro*, as
326 well as an inducer of NFAT5 activity¹⁶. The massive death of tumor cells results in hypertonicity in the
327 TME³⁹. We showed that this factor slightly affected the regulation of NFAT5 expression within the
328 tumor, but its main effect could be related to the activity of NFAT5 rather than its transcriptional
329 regulation. Our study is in line with previous observations that increased osmolarity dampens T cell
330 effector functions, unraveling another mechanism in place within the TME^{39, 46}.

331 Altogether, we uncovered a new central player in the regulation of T cell exhaustion, acting only within
332 tumors, but not during chronic infection. This discovery is particularly important in the frame of
333 adoptive cell therapy (ACT) where a patients' T cells are expanded before being transferred back into
334 the patient. Acting on NFAT5, either genetically or using specific inhibitors, would favor a stronger T
335 cell response against cancer, without decreasing the stemness capacity of transferred T cells.

336

337

338 **Figure legends**

339 **Fig. 1: NFAT5 is upregulated in tumor-infiltrating CD8 T cells.** **a)** *NFAT5* mRNA expression levels
340 in each indicated CD8 TIL subtype, as classified by ProjecTILs, across five different mouse and patient
341 cohorts/studies (CF Material and methods). **b)** Heatmap showing the activity (AUC score) of the top 8
342 TFs with the greatest difference in regulon activity (either up or down regulation) when comparing
343 terminal exhausted CD8 T cells (Tex) and naïve-like CD8 T cells (Naive like) from tumor-infiltrating T
344 lymphocytes (TILs dataset). **c)** *Nfat5* mRNA levels from CD8 T cells homing B16-gp33 tumors or
345 spleens. Ten mice pooled from two independent experiments. **d)** *NFAT5* mRNA level in human naïve
346 circulating CD8 T cells, EBV-specific CD8 T cells and ELA (Melan-A)-specific CD8 T cells from
347 tumor-infiltrated lymph nodes (TILN). **e)** mCherry levels in non-draining lymph node (N-DLN), tumor-
348 draining lymph node (T-DLN) and B16-gp33 tumors from *NFAT5*_{mCherry+/+} or *NFAT5*_{mCherry-/-} CD8 T
349 cells on day 16 post tumor injection. Four mice from one representative experiment out of two. **f)**
350 mCherry levels in N-DLN, T-DLN and MC38 tumors from *NFAT5*_{mCherry+/+} or *NFAT5*_{mCherry-/-} CD8 T
351 cells on day 16 post tumor injection. Nine mice pooled from two independent experiments. **g)** Tumor
352 growth measured in *NFAT5*_{mCherry+/+} mice transferred with OT-I-*NFAT5*_{mCherry+/+} CD8 T cells (day 7 post
353 tumor injection) or no T cell transfer (w/o transfer). **h)** mCherry expression of OT-I-*NFAT5*_{mCherry+/+}
354 (left) or endogenous- *NFAT5*_{mCherry+/+} (right) CD8 T cells from the N-DLN, T-DLN and tumor.
355 Statistical comparison between CD8 T cells from the T-DLN and tumor. **i)** mCherry expression of
356 *NFAT5*_{mCherry+/+} mice not receiving T cell transfer, TILs, T-DLN and N-DLN CD8 T cells. **g-i)** Two
357 pooled independent experiments with 9 mice per condition. **c)** Paired student t-test. **d)** Mann-Whitney
358 test. Mean. **e-i)** Two-way ANOVA. Mean with SD

359 **Fig. 2: NFAT5 overexpression dampens CD8 T cell tumor control.** **a)** *Nfat5* mRNA levels in CD8 T
360 cells transduced with a vector encoding for NFAT5 isoform A (NFAT5 A) (left) or control eGFP (right).
361 **b)** Timeline of the experiment. Activated TCRP1A CD8 T cells were transduced and transferred into
362 *Rag1*^{-/-}B10D2 mice seven days post P511 tumor engraftment. CD8 T cells were sorted for RNA-
363 sequencing on day 14. **c)** Tumor growth in mice transferred with TCRP1A CD8 T cells transduced with
364 control eGFP, NFAT5 A, or NFAT1 CA-RIT. **d)** PC analysis of CD8 TILs transduced with control

365 eGFP, NFAT5 A, or NFAT1 CA-RIT. **e)** Venn diagram showing the number of genes upregulated in
366 NFAT5 A transduced CD8 TILs, NFAT1 CA-RIT transduced TILs, or both. **f)** GO terms enriched in
367 CD8 TILs with NFAT5 A (left), or NFAT1 CA-RIT (right). **c)** Two way ANOVA. Error bars represent
368 SEM. One representative experiment out of two with 5 mice per group.

369 **Fig. 3: NFAT5 deletion in tumor-specific T cells improves tumor control.** **a)** Timeline of the
370 experiment: activated WT or NFAT5 KO P14 CD8 T cells were transferred into B16-gp33-bearing
371 CD45.1.2 mice. CD8 TILs were analyzed seven days after transfer. **b)** Tumor growth of mice transferred
372 with WT (grey) or NFAT5 KO (red) P14 CD8 T cells. In black is the control group without T cell
373 transfer. **c)** WT or NFAT5 KO P14 CD8 TILs were analyzed by flow cytometry seven days after transfer.
374 Bars represent the geometric mean. **d)** PC analysis of WT and NFAT5 KO P14 CD8 TILs. **e)** Violin
375 plots showing the distribution of upregulated (left) or downregulated (right) genes among indicated
376 tumor-infiltrating CD8 T cell subpopulations, including precursor exhausted (Tpex) and terminal
377 exhausted (Tex). **f)** Heatmap displaying 1294 genes differentially expressed in WT versus NFAT5 KO
378 P14 CD8 TILs, fold change of 1.5; adjusted p value <0.05). **g)** Genes differentially expressed in TOX
379 KO CD8 T cells were compared to genes differentially expressed in NFAT5 KO CD8 T cells using the
380 GSEA analysis. **h)** Analysis of scRNA-seq data of human melanoma tumors: Pearson correlation
381 coefficients were calculated between *NFAT5* mRNA levels and mRNA levels of indicated genes. **a-c)**
382 Seven mice per condition from one representative experiment out of three. Mann-Whitney test.

383 **Fig. 4: NFAT5 inactivation has no effect on CD8 T cell activity during chronic LCMV infection.**
384 **a)** Timeline of the experiment. WT or NFAT5 KO P14 CD8 T cells were transferred into V β 5 mice one
385 day prior LCMV clone 13 infection. **b)** The body weight of infected mice was monitored over time and
386 normalized to day 0. **c)** Flow cytometry analysis was performed 28 days after infection. Two pooled
387 experiments. Mann-Whitney test.

388 **Fig. 5: NFAT5 inactivation impacts more strongly Tpex CD8 TILs.** **a)** Fold change of P14-
389 NFAT5_{mCherry} cells over endogenous WT CD8 T cells at indicated conditions and time points for Tpex
390 (left) and Tex (right). **b)** Representative histograms of mCherry expression by P14-NFAT5_{mCherry} Tpex
391 (orange) and Tex (purple) compared to endogenous WT (dotted line) CD8 T cells at given time points

392 post LCMV clone 13 infection (left) or tumor injection (right) with quantification of mCherry⁺ T_{pex}
393 and T_{ex} at respective time points (below). One representative experiment out of two. **c)** Representative
394 histograms of mCherry expression by OT1-NFAT5_{mCherry} T_{pex} and T_{ex} at different time points post-
395 tumor injection (up) with quantification of mCherry⁺ T_{pex} and T_{ex} at respective time points (below).
396 Two independent experiments pooled. **d)** Contour plots of Slamf6 and Tim-3 expression in WT (left)
397 and NFAT5 KO (right) with the respective histograms comparing to endogenous CD8 T cells on day 28
398 post LCMV clone 13 infection. Frequencies and numbers per spleen of T_{pex} and T_{ex} in NFAT5 KO
399 and WT recipients are shown below. **e)** Immunophenotyping of T_{pex} and T_{ex} by their PD-1 expression
400 and IFN- γ production. **d-e)** One representative experiment out of three. **f)** Contour plots of Slamf6 and
401 Tim-3 expression in WT (left) and NFAT5 KO (right) with the respective histograms comparing to
402 endogenous CD8 T cells on day 14 post tumor injection (day 7 post T cell transfer). Frequencies and
403 numbers per mm³ (tumor mass) of T_{pex} and T_{ex} in NFAT5 KO and WT recipients (below). **g)**
404 Immunophenotyping of T_{pex} and T_{ex} by their PD-1 expression and IFN- γ production. Two independent
405 experiment pooled out of three. **a,b,d-g)** Mann-Whitney test. **c)** Two ways ANOVA. Bars representing
406 geometric mean.

407 **Fig. 6: NFAT5 expression is driven by TCR signaling in CD8 TILs.** **a)** mCherry levels in
408 NFAT5_{mCherry} splenocytes *ex-vivo*, after three days in culture in the presence of IL-2 (naïve) or in
409 combination with the indicated stimuli. **b)** Timeline of the experiment. Activated OT-I and P14 CD8 T
410 cells were transferred into B16-OVA and B16-gp33-bearing mice. Flow cytometry analysis seven days
411 after T cell transfer (day 16). **c)** Paired comparison of mCherry and PD-1 expression plotted as GMFI
412 of indicated TILs within B16-OVA tumors. **d)** Paired comparison of mCherry expression plotted as
413 GMFI of indicated TILs within B16-gp33 tumors. **e)** Timeline of the experiment. B16-gp33-bearing
414 mice were treated with FK506 either the first three days after T cell transfer (7 days post tumor injection)
415 or 4-6 days after T cell transfer. TILs were analyzed on day 3 and day 7 post T cell transfer. **f)** Fold
416 change of mCherry (left), PD-1 (middle) and TOX (right) between DMSO and FK506-receiving mice
417 at respective time points. Dotted line represents fold change equal to one. Two independent experiments
418 pooled. Geometric mean with error bars representing SD. **g)** Luciferase activity measured from Jurkat-

419 TonE reporter cells cultured for 24h with the indicated stimuli. **a-d, g)** One representative experiment
420 out of two. **c-d)** Paired student t-test. **f)** Mann-Whitney test.

421

422 **Extended data Fig. 1:**

423 **a)** NFAT5 reporter mouse strain: The TAG stop codon in exon 14 of the mouse *Nfat5* gene was replaced
424 by CRISPR/Cas-mediated genome engineering with the P2A-mCherry cassette to create a knock-in
425 *NFAT5-P2A-mCherry* reporter model in C57BL/6 mice. **b)** Relative expression ($2^{-\Delta\Delta Cq}$) of *mCherry*
426 and *Nfat5* assessed by RT-PCR and normalized to β -2-microglobulin of NFAT5_{mCherry+/-} or
427 NFAT5_{mCherry+/+} CD8 T cells cultured for 72h under different hyperosmolar conditions ranging from
428 300mOsm/kg to 500mOsm/kg. **c)** Histogram showing mCherry expression of NFAT5_{mCherry+/+} CD8 T
429 cells from the lymph node in comparison to a littermate control mouse (mCherry^{-/-}). **d)** Western blot
430 showing the protein level of NFAT5^{flox/flox} CD4-Cre^{-/-} (WT), CD4-Cre^{+/-} (KO) NFAT5^{flox/flox} ,
431 NFAT5_{mCherry+/-} and NFAT5_{mCherry+/+} P14 CD8 T cells cultured in complete RPMI with 1uM gp33 peptide
432 and 20U/ml rhIL-2 for 72 hours. β -actin serves as a housekeeping gene. **e-g)** Spleen (**e**), lymph node (**f**)
433 and thymus (**g**) from NFAT5_{mCherry^{-/-}}, NFAT5_{mCherry+/-} and NFAT5_{mCherry+/+} mice were collected and
434 analyzed for their immune compartment and thymic development (**g**) by flow cytometry.

435 **Extended data Fig. 2:**

436 **a)** The four murine isoforms of NFAT5 were aligned on the software Geneious using the entries from
437 genbank and Ensembl. Domains described by Cheung *et al.* were aligned against mouse isoforms 203,
438 whose length corresponds to human isoform C. NES: nuclear export signal, AD1: activation domain 1,
439 AES: auxiliary export signal, DRL: DNA recognition loop, DD: dimerization domain, RHD: rel
440 homology region, AD2: activation domain 2, AD3: activation domain 3. **b)** Gating for the sorting of
441 NFAT5 A, NFAT1 CA-RIT or control eGFP transduced CD8 T cells. **c)** Individual tumor growth per
442 mouse per group as described in Figure 2. **d)** Tumor growth comparing NFAT5 isoform A lacking the
443 DNA binding domain (DBD) (left panel) and NFAT5 isoform D (right panel) to the one of NFAT5

444 isoform A. **e)** Bioluminescence of the luciferase expressing TCRP1A CD8 T cells after injection of the
445 mice with luciferin.

446 **Extended data Fig. 3:**

447 **a)** Mean *Nfat5* expression level of various CD8 T cell populations in indicated studies assessed by
448 TILAtlas (left) and the fold change of *Nfat5* expression level of T_{pex} or T_{ex} over indicated populations
449 (right). **b)** Violin plot showing the *Nfat5* expression level (number above) in LCMV infection (left) and
450 fold change of *Nfat5* expression level of T_{pex} or T_{ex} over indicated populations (right).

451 **Extended data Fig. 4:**

452 **a)** Schematic representation of the luciferase NFAT5 activity reporter plasmid. Blue sequence represents
453 the NFAT5 (TonEBP) binding site (TonE). **b)** mCherry expression level in the spleen, T-DLN, and
454 tumor of B16-gp33 / B16-OVA-bearing mice transferred with P14-(left) and OT-I-(right)
455 NFAT5_{mCherry+/+} CD8 T cells. Two ways ANOVA. **c)** Fold change of mCherry (upper panel) or PD-1
456 (lower panel) calculated by DMSO receivers over FK506 receivers during indicated time periods in the
457 T-DLN and N-DLN. **d)** Timeline of the experiment. B16-gp33 bearing mice were transferred with either
458 KCNA3 or KCNA3 mutant overexpressing P14-NFAT5_{mCherry+/+} CD8 T cells ten days after tumor
459 injection. **e)** mCherry expression on day 17 plotted as fold change of P14 TILs over P14 CD8 T cells
460 from N-DLN.

461

462 **Materials and methods**

463

464 *Patient material*

465 To assess NFAT5 expression in human TILs by qPCR, we used amplified cDNA from Melan-A-specific
466 CD8 TILs, EBV-specific and naïve (CD8⁺CD45⁺CCR7⁺CD27⁺CD28⁺) CD8 T cells isolated from
467 healthy donor PBMCs, patient PBMCs and metastatic lymph nodes from stage III/IV metastatic
468 melanoma patients (clinical study NCT00112229)¹⁴.

469 *Animals*

470 CD45.1, CD45.1.2 and Rag1^{-/-}B10D2 TCRP1A mice were bred in house. CD45.2 CD4-Cre
471 NFAT5^{flox/flox} mice were kindly provided by Prof. Cristina López-Rodríguez⁴⁵. NFAT5-mCherry
472 reporter mice were generated by Cyagen. The TAG stop codon in exon 14 of the mouse *Nfat5* gene was
473 replaced by CRISPR/Cas-mediated genome engineering with the P2A-mCherry cassette on a C57BL/6
474 background. CD45.2 CD4-Cre NFAT5^{flox/flox} mice and NFAT5-mCherry reporter mice were crossed
475 with P14 or OT-I TCR transgenic mice and kept on a C57BL/6 background. Mice were kept in an SPF
476 animal facility. Experiments were approved by the veterinarian authorities and performed in compliance
477 with the University of Lausanne internal regulations (authorization VD2943, VD359). Tumor volume
478 was calculated with the following formula: volume [mm³] = length [mm] x width [mm] x height [mm].

479 *Cell lines*

480 Complete medium was composed of 10% heat-inactivated FBS (Gibco), penicillin/streptomycin 100
481 U/ml (Gibco), Hepes 10mM (Gibco), 1mM sodium pyruvate (Gibco) and 50μM 2-mercaptoethanol
482 (Gibco). B16-gp33²⁷ and B16-OVA were cultured in complete DMEM GlutaMAXTM-I with 100μg/ml
483 G418 (Calbiochem). P511²⁹, Jurkat and primary T cells were cultured in complete RPMI 1640
484 GlutaMAXTM-I. PlatinumE (PlatE) cells were cultured in complete DMEM with 10ug/ml Blasticidin
485 (Invivogen) and 1ug/ml Puromycin (Invivogen).

486 *Flow cytometry*

487 The following protocol was used for all tumor experiments: after the Fc receptor of the cells was blocked
488 with anti-mouse CD16/32 (Biolegend, 101320), extracellular staining was performed in FACS buffer
489 for 30 minutes. Dead cells were stained with Aqua Vivid (Invitrogen, L34966) in PBS for 15-20 minutes
490 or by adding DAPI (Thermo Fischer Scientific, D3571) directly before flow cytometry analysis. After
491 20 minutes of fixation, intracellular staining was performed for 30 minutes. The Biolegend intracellular
492 staining kit (421002) was used for cytokines and the FoxP3 staining kit (00-5523-00) was used for
493 transcription factor staining. When cytokine levels were assessed, the cells were stimulated with their
494 cognate peptide gp33 (10^{-6} M) and Golgistop (BD, 554724) for 5 hours. Antibodies are listed in
495 Extended Data Table 2.

496 *RNA extraction for sequencing / RT-qPCR*

497 Cells were centrifuged for 5 minutes at maximum speed and RNA was extracted with the RNeasy Plus
498 Micro Kit (Qiagen) following the manufacturer's recommendations. For RNA sequencing, RNA quality
499 was measured with a fragment analyzer. Reverse transcription was achieved using the High-capacity
500 cDNA Reverse Transcription kit (Applied biosystems). For qPCR, KAPA SYBR® Fast qPCR Master
501 Mix (2x) Kit (Sigma), was used. PCR amplification was performed in a 48 well plate (Illumina) on an
502 Eco machine (Illumina). Primer pairs: β 2M-F: A G A C T G A T A C A T A C G C C T G C A G, β 2M-R
503 G C A G G T T C A A A T G A A T C T T C A G, Murine NFAT5-F: G G T A C A G C C T G A A A C C C A A C, Murine
504 NFAT5-R T G C A A C A C C A C T G G T T C A T T, Human NFAT5-F: A T T G C A A A C C A A G G G A A C A,
505 Human NFAT5-R: T T G G A A T C A G G A T T T C T T C G, mCherry-F: C C C A C A A C G A G G A C T
506 A C A C C, mCherry-R: T T G T A C A G C T C G T C C A T G C C.

507

508 *Vectors*

509 NFAT1 CA-RIT (IRES-GFP) retroviral vector was obtained from Addgene (plasmid # 85181). MSCV-
510 Kcna3-Thy1.1 (pMSCV-Thy1.1:F2A:mKcna3[NM_008418.2]) and non-conducting 'pore dead'
511 construct MSGV-Kcna3-Thy1.1 (pMSCV-Thy1.1:F2A:mKcna3 W389F) (referred to as Kcna3 mutant)
512 were generated by Vector builder.

513 Cloning of the four isoforms of NFAT5: The NFAT5 coding sequences were added after an enhanced
514 GFP (eGFP) separated by the self-cleaving peptide P2A. The stop codon was removed and a FlagTag
515 sequence was added at the end of the NFAT5 sequence. The four isoforms differ in the first and last
516 exons. We first cloned the N- and C-termini of NFAT5 isoform A synthesized by Addgene into a
517 pMSGV retroviral vector. We then inserted the core murine cDNA of NFAT5 obtained on the
518 transOMIC platform to create the isoform A. We modified the first and last exon to achieve the three
519 other complete isoforms by replacing the N- and C-termini sequences by newly synthesized sequences
520 generated on GeneArt.

521 *Overexpression experiments*

522 TCRP1A CD8 T cells or P14-NFAT5_{mCherry} cells isolated from the lymph nodes. Lymphocytes were
523 activated with 1 μ g/ml of their respective peptides (P1A (LPYLGWLVF) or gp33 (KAVYNFATC)) and
524 20U/ml rhIL-2 (Proleukin Aldesleukin) one day before transduction. Viruses were produced in PlatE
525 cells as previously described ⁴⁷. Briefly, transfection of the respective plasmids was done with
526 lipofectamine 2000 (Life technologies) in DMEM. Viral supernatants were collected and filtered with
527 0.45 μ m filters (Sarstedt Ag & Co) and either used as crude supernatant or concentrated. Transduced
528 CD8 T cells were injected i.v. (5×10^6) into tumor-bearing hosts one day post transduction. For NFAT5
529 overexpression, eGFP positive sorted cells were collected and injected i.v. into tumor-bearing mice
530 (minimum 1×10^4 transduced cells per mouse). To follow CD8 T cell infiltration, mice were injected
531 intraperitoneal with 3mg of luciferin (Biosynth, L-8220), anesthetized with isoflurane (about 4% in air)
532 and bioluminescence was captured with an IVIS LUMINA II machine. P511 tumors were cut into pieces
533 and digested with 1mg/ml collagenase I and 100 μ g/ml DNase (Sigma) for 30 minutes at 37°C. Tumors
534 were passed through a 70 μ m cell strainer (Falcon). T cells from P511 were isolated with a Ficoll gradient
535 (Fresenius Kabi Norge AS).

536 *T cell transfer experiments in tumor-bearing mice (B16-gp33 and B16-OVA)*

537 LN cell suspensions were cultured in complete RPMI + 1 μ g/ml gp33 peptide (KAVYNFATC) or
538 1 μ g/ml Ovalbumin peptide (SIINFEKL) + 20U/ml rhIL-2 (Proleukin Aldesleukin) for two days. CD8
539 T cells were counted and resuspended into PBS before i.v. injection (5×10^6 cells/mouse). On the day of

540 the analysis, tumors were collected in complete RPMI and passed through 70 μ m cell strainers (Falcon).
541 T cells from tumors were isolated with a 40/70 percoll gradient (VWR 17-0891). When sorted for RNA
542 sequencing, the cells were collected in RNA later (Invitrogen).

543 *T cell transfer in LCMV-infected mice*

544 V β 5 mice were infected with 2x10⁶ PFU one day after transfer of 1x10³ P14 WT or NFAT5 KO P14
545 CD8 T cells. To stimulate cells for cytokine staining, cells were incubated 30 minutes with 1 μ M gp33
546 before addition of 5 μ g/ml of brefeldin A (Biolegend). The cells were then incubated 4 hours 30 minutes
547 before staining.

548 *Jurkat TonE-NFAT5 reporter*

549 Jurkat-TonE was generated by lentiviral transduction of Jurkat cells with a plasmid encoding for
550 luciferase under the control of 2x TonE promoter. 5x10⁵ reporter-expressing Jurkat cells were plated in
551 a 96-well plate and cultured for 24 hours with complete RPMI supplemented with the indicated (10ng
552 PMA (Sigma-Aldrich) / 200ng ionomycin (Thermo Fisher), for mouse 10 μ g/mL CD3 (OKT3 -
553 eBioscience)/CD28 (CD28.2 – eBioscience), ROS: 10 μ M Butyl-Hydroperoxid, 10ng/mL TGF- β
554 (Roche), 0,5% O₂ or NaCl / KCl as indicated)..

555 *Statistical and bioinformatic analyses*

556 Statistical analyses were performed with Graphpad Prism version 9. Statistical tests are indicated in the
557 legends. Comparisons of more than two groups and subsequent p-values were calculated by ANOVAs
558 with corrections as needed and specified below the figures. A p-value of <0.05 was used as the threshold
559 to define statistical significance.

560 *RNA-seq-Transcript quantification.*

561 Transcript abundance quantification was performed with Salmon 0.14.1⁴⁸ in quasi-mapping-based
562 mode using the mouse reference transcriptome (assembly GRCm38.p2) obtained from ENSEMBLE⁴⁹.
563 Default parameters were used plus the --seqBias, --gcBias, --validateMappings, --fldMean 200 and –
564 fldSD 30 parameters.

565 *Differential expression analyses.*

566 Differential gene expression analyses were performed using DESeq2 1.24.0⁵⁰. Transcript-level
567 abundances were summarized at the gene level using tximport 1.12.3⁵¹. Genes with low read counts
568 were filtered out (requiring genes to have a count of at least 10 in at least a number of samples equal to
569 the smallest group size). Overall similarity between samples was assessed by first applying a regularized
570 stabilizing transformation (rlog) to the gene-level count matrices using the *rlog* function, and then
571 performing a principal components analysis (PCA) on the regularized matrix using the *plotPCA*
572 function. Significant genes were identified using a false discovery rate (FDR) threshold of 5% and an
573 absolute log₂ fold change threshold of 1.5. The GO term analysis were performed with the EnrichR
574 platform^{52, 53} using the “GO Biological Process 2018” algorithm. Enrichment of the NFAT5 KO
575 differentially expressed gene set in TOX up or downregulated genes was evaluated using the TOX
576 expression data published in³⁴, available from the Gene Expression Omnibus (GEO) database under
577 accession number GSE126973. NFAT5 KO differentially expressed genes were ranked based on the
578 log₂ fold change (ranked list), and TOX signatures of up or down gene regulation were created based
579 on TOX knockout differentially expressed genes with positive or negative log₂ fold change. Enrichment
580 scores and adjusted p-values were computed using the *fgsea* function and the ranked list and regulation
581 signatures mentioned above, with the number of permutations set to 1,000. Enrichment plots were
582 obtained using the *plotEnrichment* function.

583 *TIL atlas*

584 The TIL atlas dataset used in Fig.1a, b and Extended data Fig.3, which includes 16,803 high-quality
585 single-cell transcriptomes from 25 samples (B16 melanoma and MC38 colon adenocarcinoma tumors)
586 from six different studies, has been collected, thoroughly analyzed and annotated by Andreatta and co-
587 workers²⁶, and it is publicly available (<https://doi.org/10.6084/m9.figshare.12478571>).

588 *Regulon analysis of tumor-infiltrating T lymphocyte*

589 Regulons (gene sets regulated by the same transcription factor) and their activity were inferred and
590 evaluated using the SCENIC pipeline (<https://scenic.aertslab.org>)⁵⁴, which can be described in three

591 steps. Step 1) Infer gene regulatory network (GRN) using grnBoost2, which is a faster implementation
592 of the original algorithm Genie3⁵⁵; scRNA-seq transcriptomics data is used as the input to infer causality
593 from the expression levels of the transcription factors to the targets based on co-expression patterns. The
594 importance of each transcription factor in the prediction of the target gene expression pattern is taken as
595 an indication of a putative regulatory event. The aggregation of the top 50 targets per TF and the top 5
596 TF per target was used to define raw putative regulons. Step 2) Co-expression modules (raw putative
597 regulons, i.e. sets of genes regulated by the same transcription factor) derived from the GRN generated
598 in Step 1 are refined by pruning indirect targets by motif discovery analysis using cisTarget algorithm
599 and a cis-regulatory motif database^{56, 57}. We used mm9-500bp-upstream-7species.mc9nr.feather and
600 mm9-tss-centered-10kb-7species.mc9nr.feather databases. The motif database includes a score for each
601 pair motif-gene, so that a motif-gene ranking can be derived. A motif enrichment score is then calculated
602 for the list of transcription factor selected targets by calculating the Area Under the recovery Curve
603 (AUC) on the motif-gene ranking 1 using the RcisTarget R package
604 (<https://github.com/aertslab/RcisTarget>). If a motif is enriched among the list of transcription factor
605 targets, a regulon is derived including the target genes with a high motif-gene score. Step 3) evaluation
606 of regulon activity of each individual cell using AUCell (<https://github.com/aertslab/AUCell>), which
607 provides an AUC score for each regulon; we discarded regulons with less than 5 constituent elements,
608 as the estimation of the activity of small regulons is less reliable. In order to compare the regulon activity
609 profile of CD8 exhausted T cells and CD8 naïve cells from the TILs dataset, we used the regulon activity
610 (AUC score) matrix and performed, for each regulon, a Wilcoxon Rank Sum test implemented within
611 the FindMarkers function of the SEURAT R package (version 4.0.3). Only regulons with an adjusted p-
612 value for this test of 0.05 or less were considered as differentially active (Bonferroni correction).

613

614 *Evaluation of NFAT5 KO signature in tumor-infiltrating T lymphocytes*

615 Differentially expressed genes up (n=458) and down (n=832) regulated from the comparison
616 NFAT5.KO Vs. WT were considered separately as two different signatures to be analyzed in the TILs
617 dataset (NFAT5.KO.DEG.UP and NFAT5.KO.DEG.DOWN, respectively). The AUCell R package⁵⁴

618 was used to evaluate these signatures across tumor-infiltrating T lymphocyte subpopulations using the
619 normalized gene expression matrix of this dataset.

620 *Western Blot*

621 NFAT5^{lox/lox} CD4-Cre^{-/-} (WT), CD4-Cre^{+/-} (KO) NFAT5^{lox/lox}, NFAT5^{mCherry +/-} and NFAT5^{mCherry +/+}
622 P14 CD8 T cells were cultured in complete RPMI with 1 μ M gp33 peptide and 20U/ml rhIL-2 (Proleukin
623 Aldesleukin) for 72 hours. Whole cell extracts were isolated using RIPA lysis buffer (25mM Tris HCl
624 pH 7.6, 150mM NaCl, 1% NP 40, 1% sodium deoxychlorate, 0,1% SDS; Cell Signaling Technology)
625 supplemented with DNase, 1x phosphatase inhibitor (PhosSTOP Roche) and 1x protease inhibitor
626 (complete protease inhibitor cocktail Roche). Protein concentration was assessed by the Bradford Assay
627 (Biorad Protein Assay Kit II) and 25ug of cell lysates from each condition were resolved by 8% SDS-
628 PAGE with NuPAGE electrophoresis system (Invitrogen/Thermo Fisher Scientific). Proteins were then
629 transferred to PVDF membrane (Invitrogen/Thermo Fisher Scientific) by Trans-Blot SD semidry
630 transfer cell (Bio-Rad) at 18 V for 30 minutes. Membranes were blocked with 5% w/v nonfat dry milk
631 (Sigma-Aldrich) and then incubated with the indicated primary antibodies at 4 °C overnight. The bands
632 were visualized using Thermo Scientific™ Pierce™ ECL Western Blotting Substrate after incubation
633 with horseradish peroxidase (HRP)-conjugated antibodies for 1 hour at room temperature. Primary
634 antibodies: anti-NFAT5 antibody (Santa Cruz) and anti-beta-actin antibody (Invitrogen).

635

636

637

638

639

640

641

642 References

- 643 1. Blank, C.U. *et al.* Defining 'T cell exhaustion'. *Nat Rev Immunol* **19**, 665-674 (2019).
644
645 2. Utzschneider, D.T. *et al.* High antigen levels induce an exhausted phenotype in a chronic
646 infection without impairing T cell expansion and survival. *J Exp Med* **213**, 1819-1834 (2016).
647
648 3. Speiser, D.E., Ho, P.C. & Verdeil, G. Regulatory circuits of T cell function in cancer. *Nat Rev*
649 *Immunol* **16**, 599-611 (2016).
650
651 4. Ribas, A. & Wolchok, J.D. Cancer immunotherapy using checkpoint blockade. *Science* **359**,
652 1350-+ (2018).
653
654 5. Cheng, H., Ma, K., Zhang, L. & Li, G. The tumor microenvironment shapes the molecular
655 characteristics of exhausted CD8(+) T cells. *Cancer Lett* **506**, 55-66 (2021).
656
657 6. Siddiqui, I. *et al.* Intratumoral Tcf1(+)PD-1(+)CD8(+) T Cells with Stem-like Properties Promote
658 Tumor Control in Response to Vaccination and Checkpoint Blockade Immunotherapy.
659 *Immunity* **50**, 195-211 e110 (2019).
660
661 7. Alfei, F. *et al.* TOX reinforces the phenotype and longevity of exhausted T cells in chronic viral
662 infection. *Nature* **571**, 265-269 (2019).
663
664 8. Yao, C. *et al.* Single-cell RNA-seq reveals TOX as a key regulator of CD8(+) T cell persistence in
665 chronic infection. *Nat Immunol* **20**, 890-901 (2019).
666
667 9. Khan, O. *et al.* TOX transcriptionally and epigenetically programs CD8(+) T cell exhaustion.
668 *Nature* **571**, 211-218 (2019).
669
670 10. Seo, H. *et al.* TOX and TOX2 transcription factors cooperate with NR4A transcription factors
671 to impose CD8(+) T cell exhaustion. *Proc Natl Acad Sci U S A* **116**, 12410-12415 (2019).
672
673 11. Hogan, P.G., Chen, L., Nardone, J. & Rao, A. Transcriptional regulation by calcium, calcineurin,
674 and NFAT. *Genes Dev* **17**, 2205-2232 (2003).
675
676 12. Klein-Hessling, S. *et al.* NFATc1 controls the cytotoxicity of CD8(+) T cells. *Nat Commun* **8**, 511
677 (2017).
678
679 13. Martinez, G.J. *et al.* The transcription factor NFAT promotes exhaustion of activated CD8(+) T
680 cells. *Immunity* **42**, 265-278 (2015).
681
682 14. Baitsch, L. *et al.* Exhaustion of tumor-specific CD8(+) T cells in metastases from melanoma
683 patients. *J Clin Invest* **121**, 2350-2360 (2011).

- 684
685 15. Lopez-Rodriguez, C., Aramburu, J., Rakeman, A.S. & Rao, A. NFAT5, a constitutively nuclear
686 NFAT protein that does not cooperate with Fos and Jun. *Proc Natl Acad Sci U S A* **96**, 7214-
687 7219 (1999).
- 688
689 16. Cheung, C.Y. & Ko, B.C. NFAT5 in cellular adaptation to hypertonic stress - regulations and
690 functional significance. *J Mol Signal* **8**, 5 (2013).
- 691
692 17. Aramburu, J. & Lopez-Rodriguez, C. Regulation of Inflammatory Functions of Macrophages
693 and T Lymphocytes by NFAT5. *Front Immunol* **10**, 535 (2019).
- 694
695 18. Tellechea, M., Buxade, M., Tejedor, S., Aramburu, J. & Lopez-Rodriguez, C. NFAT5-Regulated
696 Macrophage Polarization Supports the Proinflammatory Function of Macrophages and T
697 Lymphocytes. *J Immunol* **200**, 305-315 (2018).
- 698
699 19. Kim, N.H. *et al.* Reactive oxygen species regulate context-dependent inhibition of NFAT5
700 target genes. *Exp Mol Med* **45**, e32 (2013).
- 701
702 20. Alberdi, M. *et al.* Context-dependent regulation of Th17-associated genes and IFNgamma
703 expression by the transcription factor NFAT5. *Immunol Cell Biol* (2016).
- 704
705 21. Carmona, S.J., Siddiqui, I., Bilous, M., Held, W. & Gfeller, D. Deciphering the transcriptomic
706 landscape of tumor-infiltrating CD8 lymphocytes in B16 melanoma tumors with single-cell
707 RNA-Seq. *Oncoimmunology* **9**, 1737369 (2020).
- 708
709 22. Xiong, H. *et al.* Coexpression of Inhibitory Receptors Enriches for Activated and Functional
710 CD8(+) T Cells in Murine Syngeneic Tumor Models. *Cancer Immunol Res* **7**, 963-976 (2019).
- 711
712 23. Jerby-Arnon, L. *et al.* A Cancer Cell Program Promotes T Cell Exclusion and Resistance to
713 Checkpoint Blockade. *Cell* **175**, 984-997 e924 (2018).
- 714
715 24. Sade-Feldman, M. *et al.* Defining T Cell States Associated with Response to Checkpoint
716 Immunotherapy in Melanoma. *Cell* **175**, 998-1013 e1020 (2018).
- 717
718 25. Azizi, E. *et al.* Single-Cell Map of Diverse Immune Phenotypes in the Breast Tumor
719 Microenvironment. *Cell* **174**, 1293-1308 e1236 (2018).
- 720
721 26. Andreatta, M. *et al.* Interpretation of T cell states from single-cell transcriptomics data using
722 reference atlases. *Nat Commun* **12**, 2965 (2021).
- 723
724 27. Prevost-Blondel, A. *et al.* Tumor-infiltrating lymphocytes exhibiting high ex vivo cytolytic
725 activity fail to prevent murine melanoma tumor growth in vivo. *J Immunol* **161**, 2187-2194
726 (1998).
- 727

- 728 28. Van den Eynde, B., Mazarguil, H., Lethe, B., Laval, F. & Gairin, J.E. Localization of two
729 cytotoxic T lymphocyte epitopes and three anchoring residues on a single nonameric peptide
730 that binds to H-2Ld and is recognized by cytotoxic T lymphocytes against mouse tumor P815.
731 *Eur J Immunol* **24**, 2740-2745 (1994).
- 732
- 733 29. Shanker, A. *et al.* CD8 T cell help for innate antitumor immunity. *J Immunol* **179**, 6651-6662
734 (2007).
- 735
- 736 30. Giordano, M. *et al.* Molecular profiling of CD8 T cells in autochthonous melanoma identifies
737 Maf as driver of exhaustion. *EMBO J* **34**, 2042-2058 (2015).
- 738
- 739 31. Giordano, M. *et al.* The tumor necrosis factor alpha-induced protein 3 (TNFAIP3, A20)
740 imposes a brake on antitumor activity of CD8 T cells. *Proc Natl Acad Sci U S A* **111**, 11115-
741 11120 (2014).
- 742
- 743 32. Chen, J. *et al.* NR4A transcription factors limit CAR T cell function in solid tumours. *Nature*
744 **567**, 530-534 (2019).
- 745
- 746 33. Berga-Bolanos, R., Alberdi, M., Buxade, M., Aramburu, J. & Lopez-Rodriguez, C. NFAT5
747 induction by the pre-T-cell receptor serves as a selective survival signal in T-lymphocyte
748 development. *Proc Natl Acad Sci U S A* **110**, 16091-16096 (2013).
- 749
- 750 34. Scott, A.C. *et al.* TOX is a critical regulator of tumour-specific T cell differentiation. *Nature*
751 **571**, 270-274 (2019).
- 752
- 753 35. Tirosh, I. *et al.* Dissecting the multicellular ecosystem of metastatic melanoma by single-cell
754 RNA-seq. *Science* **352**, 189-196 (2016).
- 755
- 756 36. Wherry, E.J. *et al.* Molecular signature of CD8+ T cell exhaustion during chronic viral
757 infection. *Immunity* **27**, 670-684 (2007).
- 758
- 759 37. Alam, S.M. *et al.* Qualitative and quantitative differences in T cell receptor binding of agonist
760 and antagonist ligands. *Immunity* **10**, 227-237 (1999).
- 761
- 762 38. Boulter, J.M. *et al.* Potent T cell agonism mediated by a very rapid TCR/pMHC interaction. *Eur*
763 *J Immunol* **37**, 798-806 (2007).
- 764
- 765 39. Eil, R. *et al.* Ionic immune suppression within the tumour microenvironment limits T cell
766 effector function. *Nature* **537**, 539-543 (2016).
- 767
- 768 40. Kumar, R. *et al.* NFAT5, which protects against hypertonicity, is activated by that stress via
769 structuring of its intrinsically disordered domain. *Proc Natl Acad Sci U S A* **117**, 20292-20297
770 (2020).
- 771

- 772 41. Brand, A. *et al.* LDHA-Associated Lactic Acid Production Blunts Tumor Immunosurveillance by
773 T and NK Cells. *Cell Metab* **24**, 657-671 (2016).
- 774
775 42. Ho, P.C. *et al.* Phosphoenolpyruvate Is a Metabolic Checkpoint of Anti-tumor T Cell
776 Responses. *Cell* **162**, 1217-1228 (2015).
- 777
778 43. Voutouri, C. & Stylianopoulos, T. Evolution of osmotic pressure in solid tumors. *J Biomech* **47**,
779 3441-3447 (2014).
- 780
781 44. Buxade, M. *et al.* Gene expression induced by Toll-like receptors in macrophages requires the
782 transcription factor NFAT5. *J Exp Med* **209**, 379-393 (2012).
- 783
784 45. Drews-Elger, K., Ortells, M.C., Rao, A., Lopez-Rodriguez, C. & Aramburu, J. The transcription
785 factor NFAT5 is required for cyclin expression and cell cycle progression in cells exposed to
786 hypertonic stress. *PLoS One* **4**, e5245 (2009).
- 787
788 46. Vodnala, S.K. *et al.* T cell stemness and dysfunction in tumors are triggered by a common
789 mechanism. *Science* **363** (2019).
- 790
791 47. Verdeil, G., Puthier, D., Nguyen, C., Schmitt-Verhulst, A.M. & Auphan-Anezin, N. STAT5-
792 mediated signals sustain a TCR-initiated gene expression program toward differentiation of
793 CD8 T cell effectors. *J Immunol* **176**, 4834-4842 (2006).
- 794
795 48. Patro, R., Duggal, G., Love, M.I., Irizarry, R.A. & Kingsford, C. Salmon provides fast and bias-
796 aware quantification of transcript expression. *Nat Methods* **14**, 417-419 (2017).
- 797
798 49. Hunt, S.E. *et al.* Ensembl variation resources. *Database (Oxford)* **2018** (2018).
- 799
800 50. Love, M.I., Huber, W. & Anders, S. Moderated estimation of fold change and dispersion for
801 RNA-seq data with DESeq2. *Genome Biol* **15**, 550 (2014).
- 802
803 51. Sonesson, C., Love, M.I. & Robinson, M.D. Differential analyses for RNA-seq: transcript-level
804 estimates improve gene-level inferences. *F1000Res* **4**, 1521 (2015).
- 805
806 52. Kuleshov, M.V. *et al.* Enrichr: a comprehensive gene set enrichment analysis web server 2016
807 update. *Nucleic Acids Res* **44**, W90-97 (2016).
- 808
809 53. Chen, E.Y. *et al.* Enrichr: interactive and collaborative HTML5 gene list enrichment analysis
810 tool. *BMC Bioinformatics* **14**, 128 (2013).
- 811
812 54. Aibar, S. *et al.* SCENIC: single-cell regulatory network inference and clustering. *Nat Methods*
813 **14**, 1083-1086 (2017).

- 815 55. Huynh-Thu, V.A., Irrthum, A., Wehenkel, L. & Geurts, P. Inferring regulatory networks from
816 expression data using tree-based methods. *PLoS One* **5** (2010).
- 817
818 56. Herrmann, C., Van de Sande, B., Potier, D. & Aerts, S. i-cisTarget: an integrative genomics
819 method for the prediction of regulatory features and cis-regulatory modules. *Nucleic Acids*
820 *Res* **40**, e114 (2012).
- 821
822 57. Imrichova, H., Hulselmans, G., Atak, Z.K., Potier, D. & Aerts, S. i-cisTarget 2015 update:
823 generalized cis-regulatory enrichment analysis in human, mouse and fly. *Nucleic Acids Res* **43**,
824 W57-64 (2015).
- 825
826

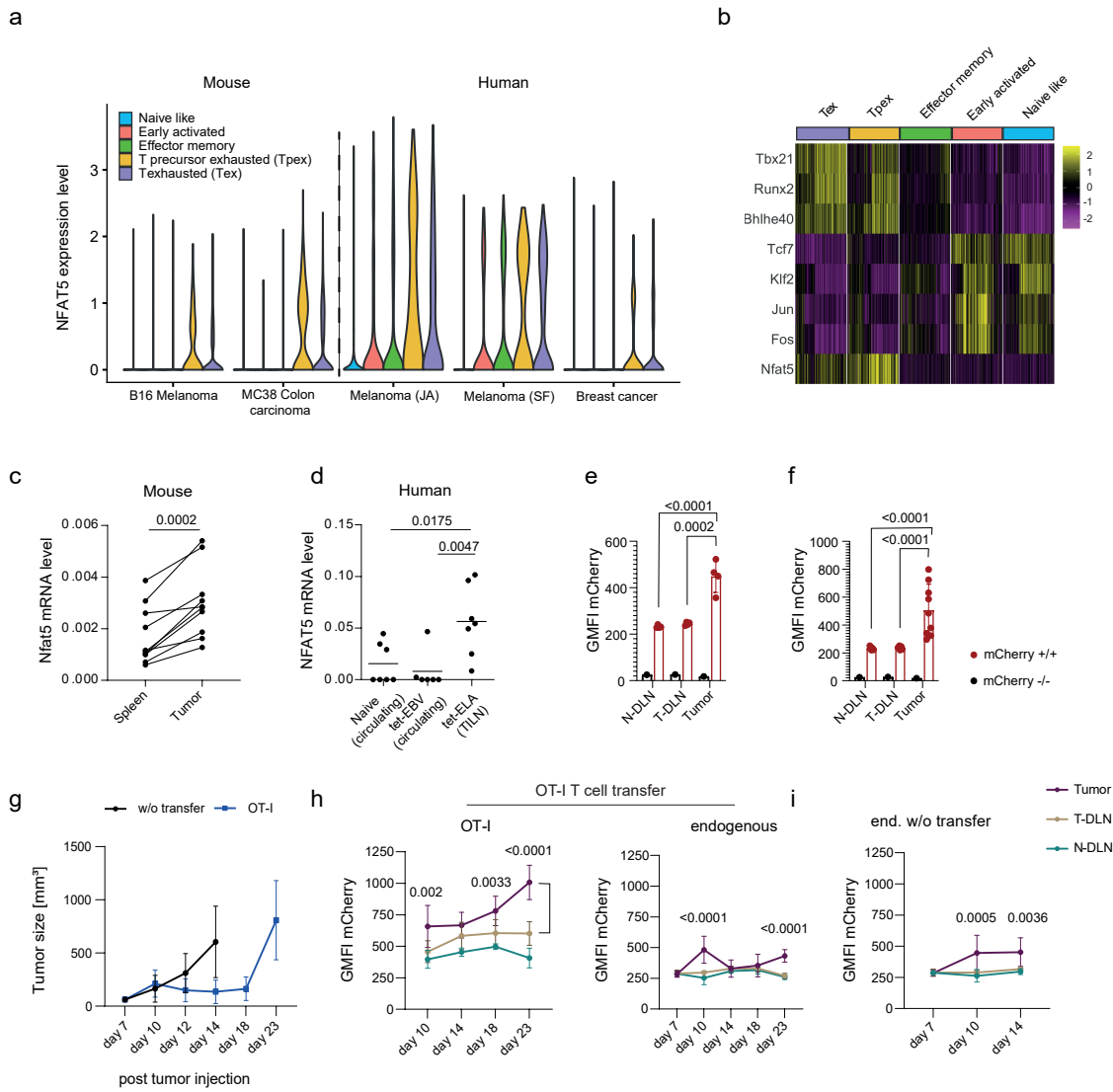


Figure 1

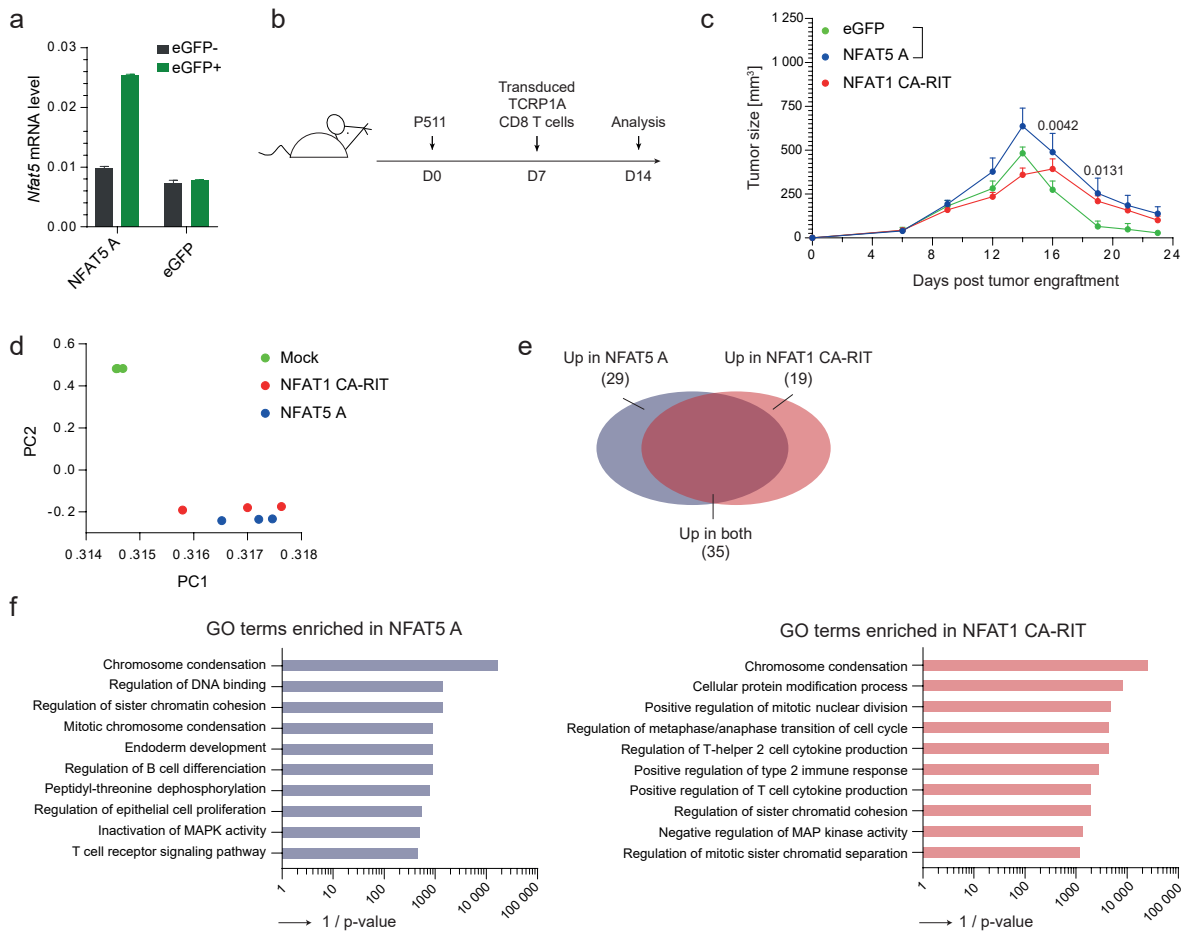


Figure 2

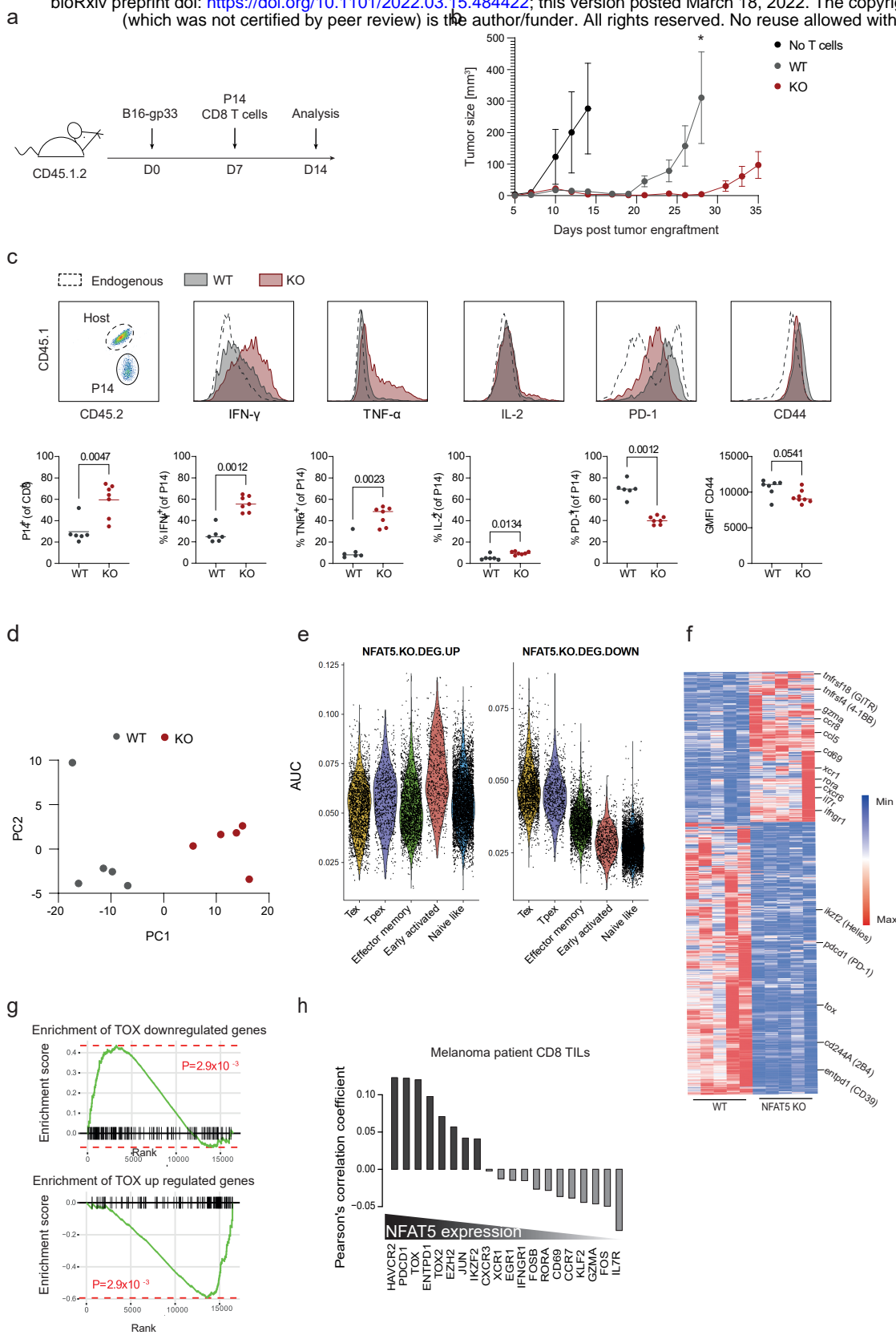


Figure 3

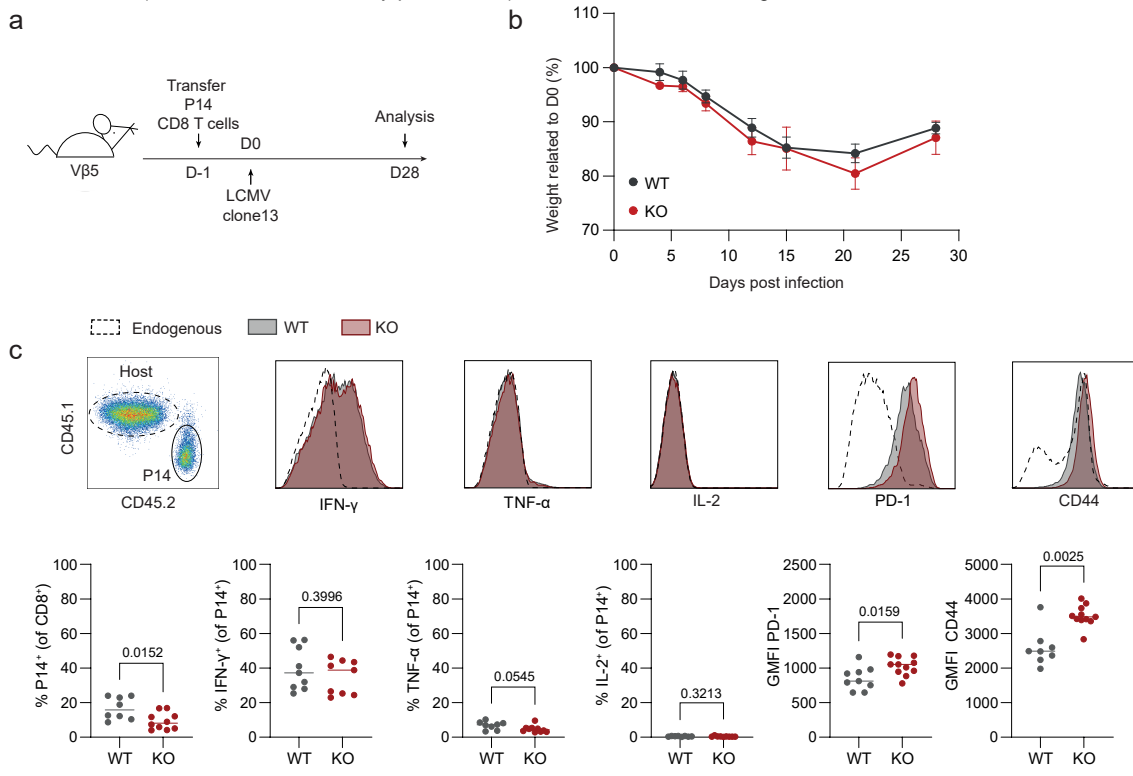


Figure 4

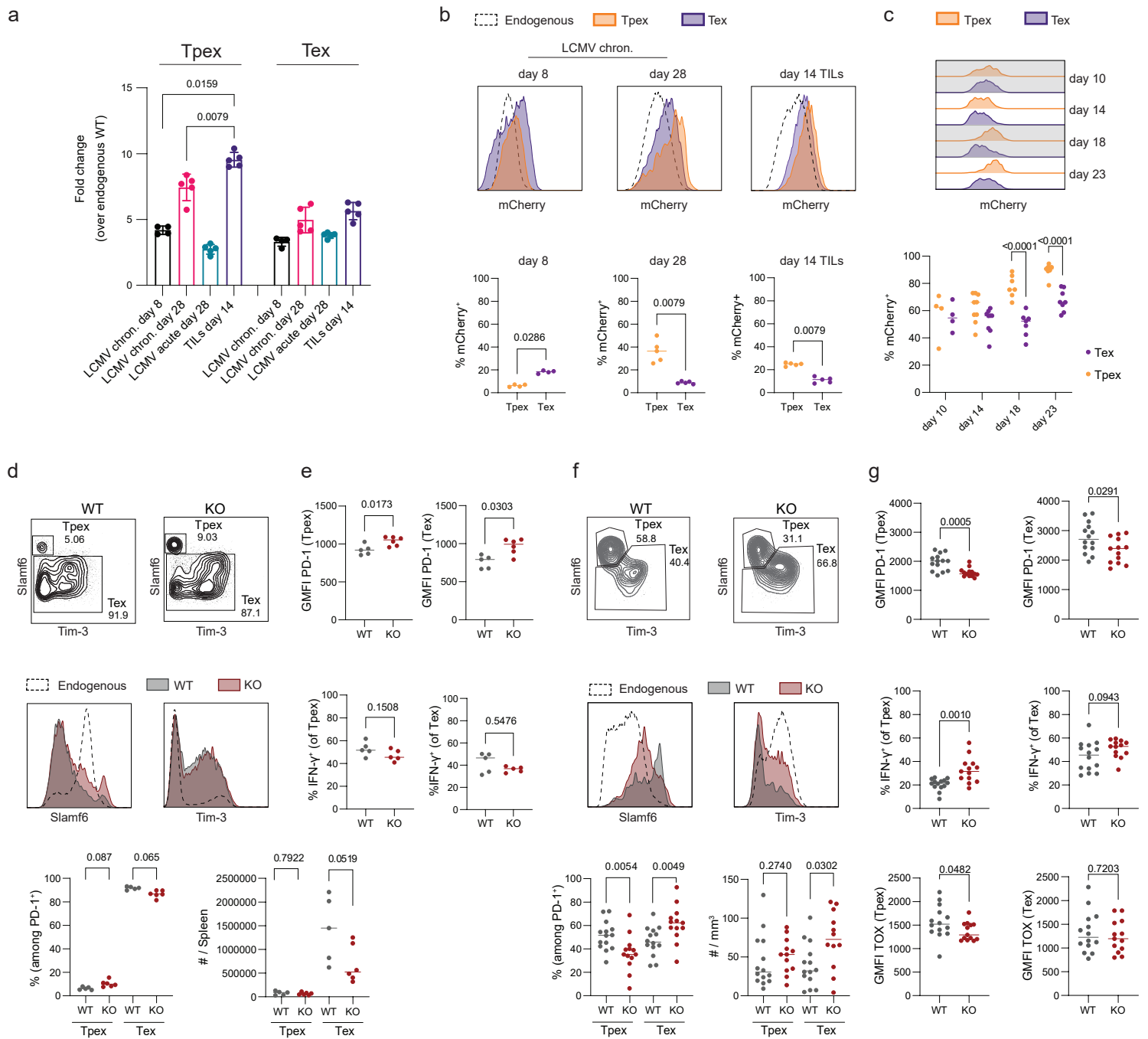


Figure 5

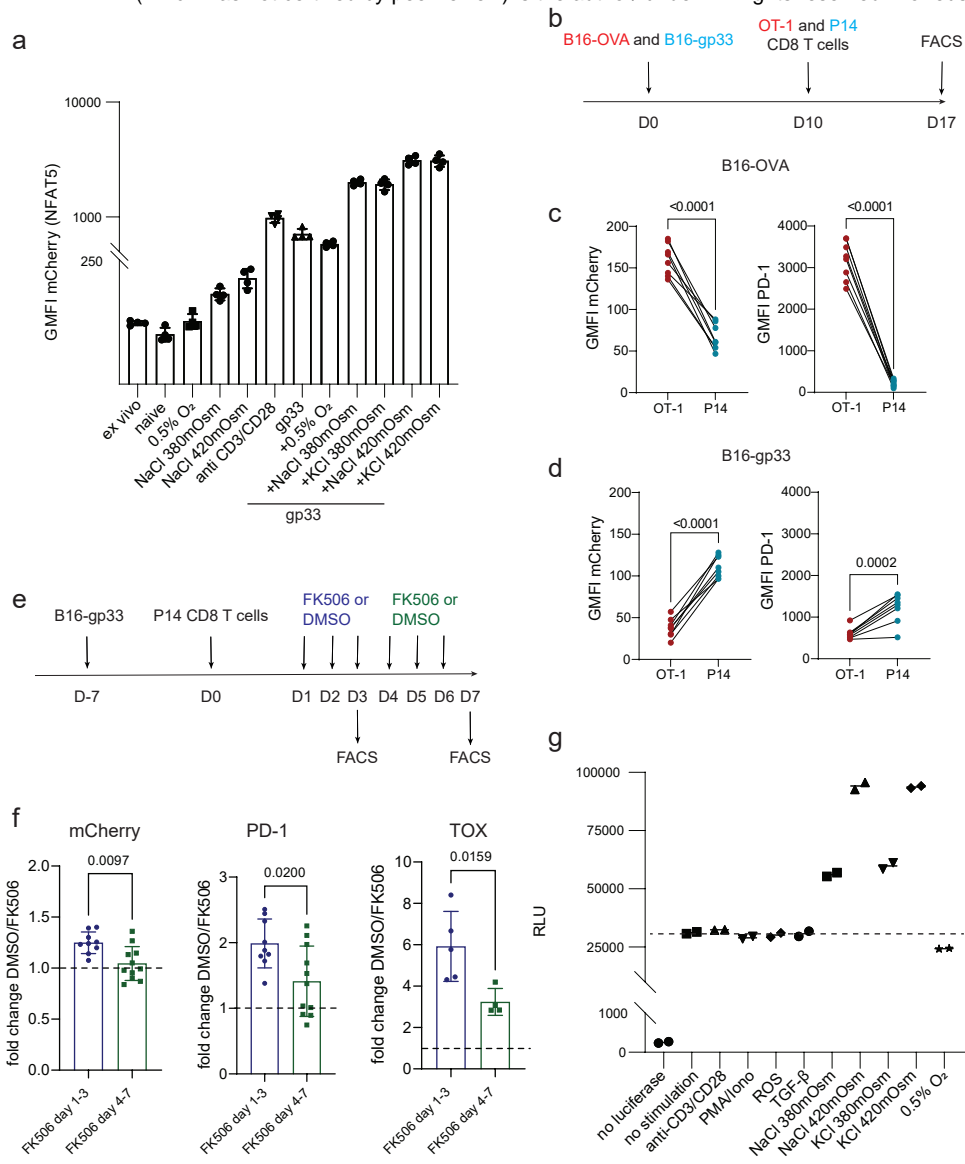
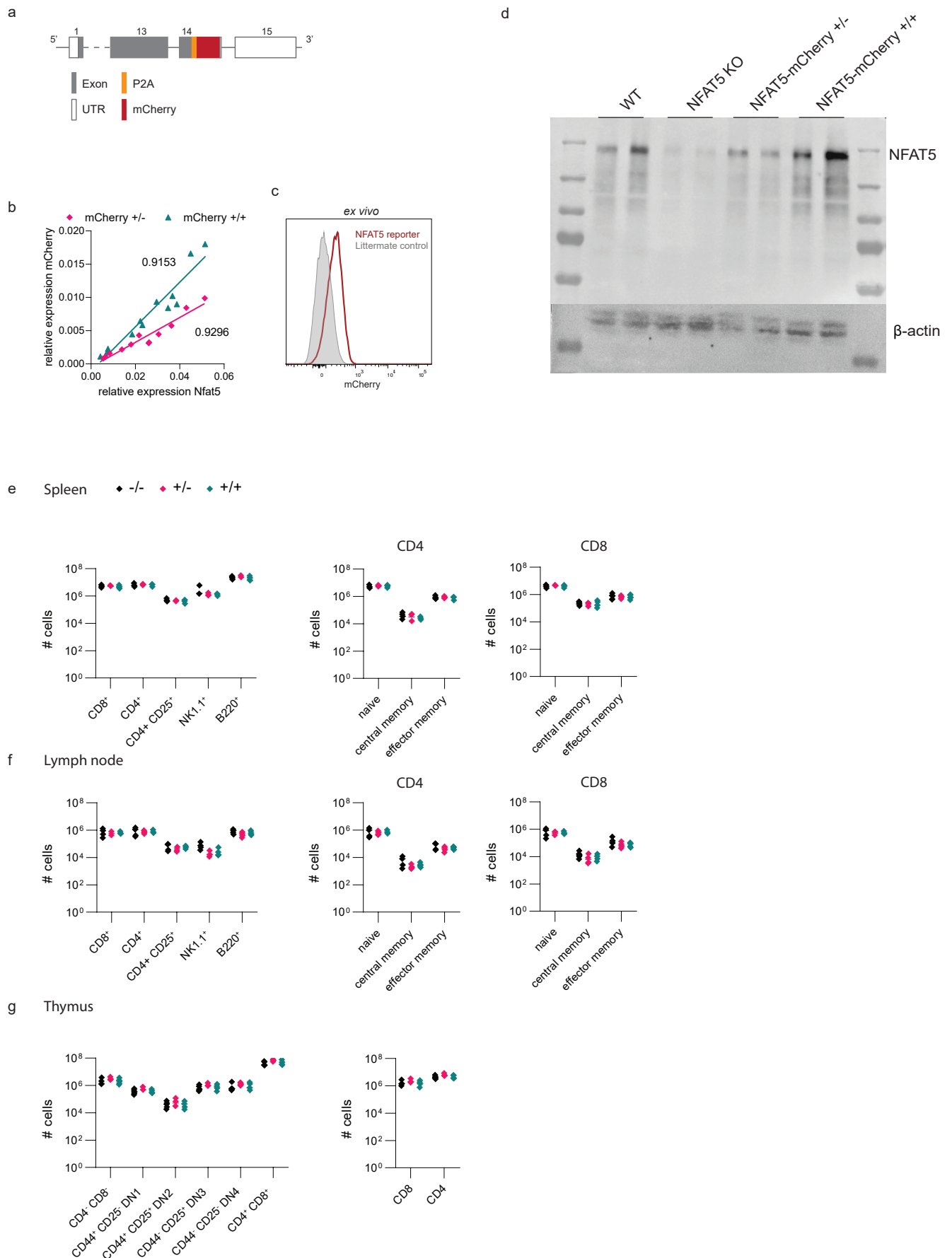
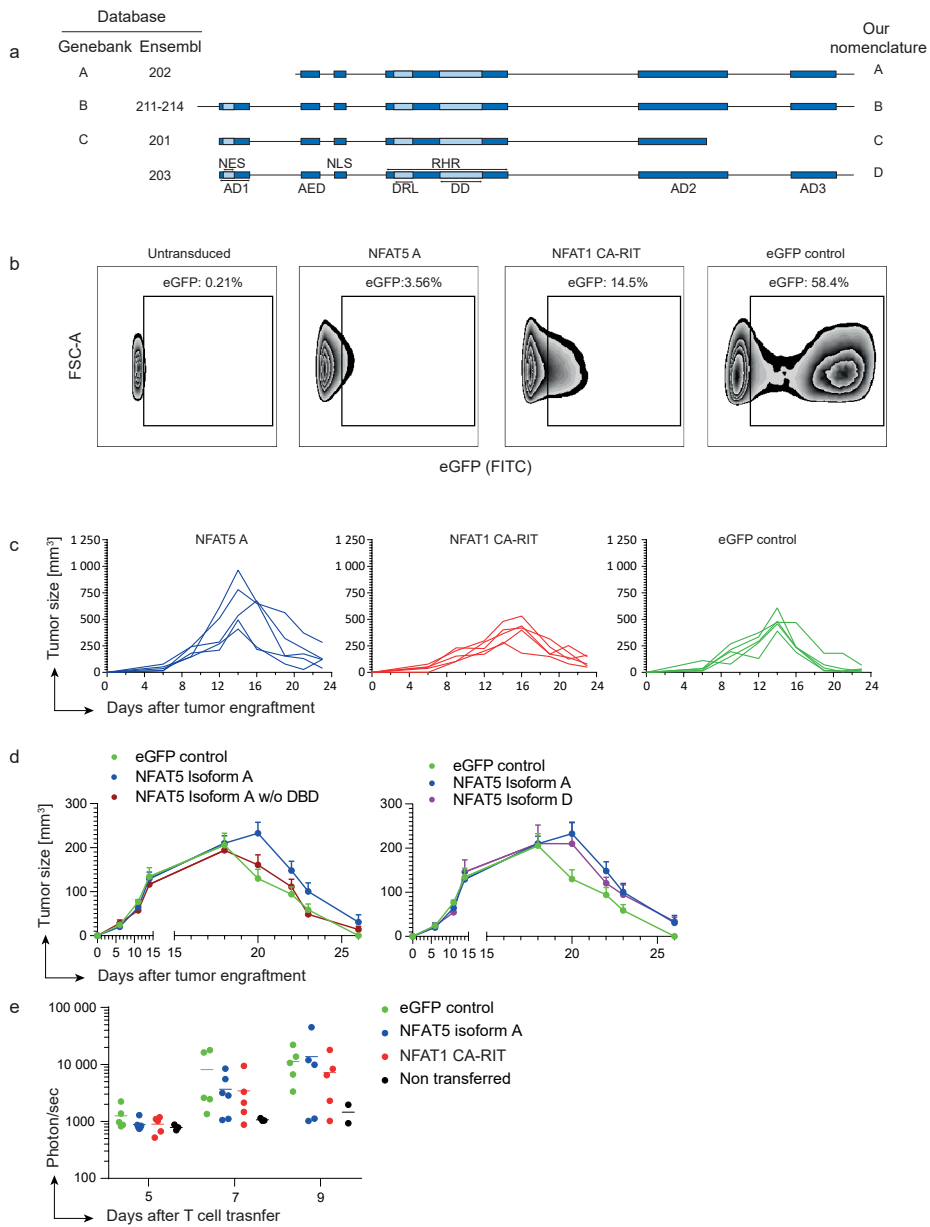


Figure 6

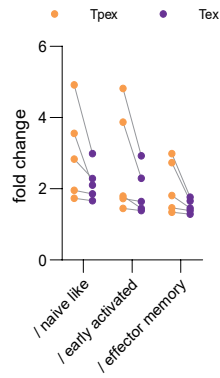




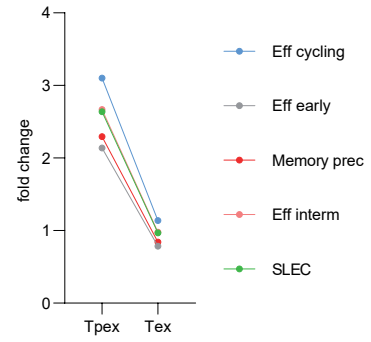
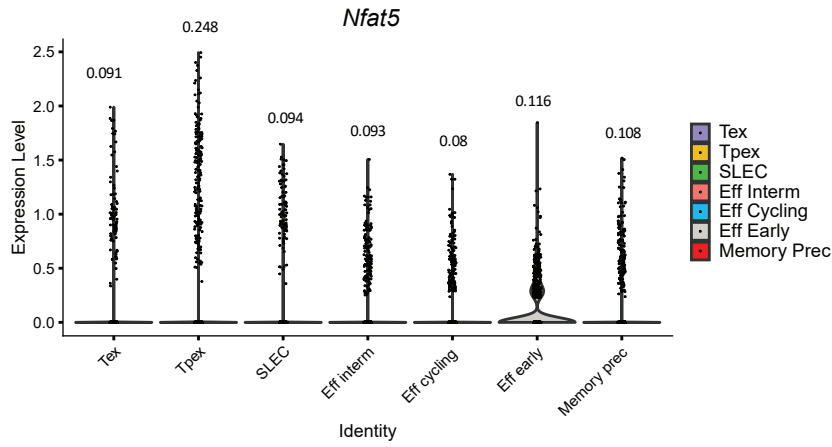
Extended data 2

a

	M_B16	M_MC38	H_Mel_JArmon	H_Mel_SFeldman	H_BrC_Azizi
CD8_NaiveLike	0.07	0.16	0.36	0.41	0.16
CD8_EarlyActiv	0.07	0.15	0.56	0.47	0.19
CD8_EffectorMemory	0.12	0.19	0.56	0.55	0.21
CD8_Tpex	0.33	0.57	1.01	0.80	0.28
CD8_Tex	0.20	0.34	0.82	0.77	0.27



b



Extended data 3

